Contents - J through K

ROSINA'S FIRST MEASUREMENTS FROM SPACE AND ANTICIPATED ANALYSES AT COMET CHURYUMOV-GERASIMENKO. A. Jäckel[1], K. Altwegg[1], P. Wurz[1], H. Balsiger[1], E. Arijs[2], J. J. Berthelier[3], S. Fuselier[4], F. Gliem[5], T. Gombosi[6], A. Korth[7], and H. Rème[8], [1]Physikalisches Institut, Universität Bern, Sidlerstr. 5, CH-3012 Bern (jaeckel@phim.unibe.ch), [2]Belgisch Instituut voor Ruimte-Aeronomie, B-1180 Brussel, [3]Institute Pierre Simon Laplace, F-94107 St.-Maur-des-Fossés, [4]Lockheed Martin Advanced Technology Center, Palo Alto, CA 94304, USA, [5]University of Michigan, Space Physics Research Laboratory, Ann Arbor, MI 48109, USA, [6]Max-Planck-Institut für Sonnensystemforschung, D-37191 Katlenburg-Lindau, [7]Centre d'Etude Spatiale des Rayonnements, F-31028 Toulouse.

Introduction: The Rosetta Orbiter Spectrometer for Ion and Neutral Analysis (ROSINA) is an orbiter payload instrument onboard the ROSETTA spacecraft that was successfully launched in March 2004 by the European Space Agency. The ROSINA instrument package is designed to determine the elemental, isotopic, and molecular composition of the atmosphere of comet 67P/Churyumov-Gerasimenko.

ROSINA Characteristics: The instrument package ROSINA consists of two mass spectrometers and one pressure sensor. The mass spectrometers are the Double Focussing Mass Spectrometer (DFMS) and the Reflectron Time-Of-Flight mass spectrometer (RTOF) that are both designed to analyze cometary neutral gases and cometary ions. The third sensor, the COmetary Pressure Sensor (COPS), consists of a pressure gauge assembly. These three sensors will measure the neutral gas and the ion composition in the cometary environment as a function of the heliocentric distance to the comet [1]. The Data Processing Unit (DPU) controls all three sensors and is fully redundant. The characteristic features of the three sensors are described in more detail below:

DFMS. The DFMS is a very compact state of the art high-resolution double-focussing mass spectrometer [2] realized in the Nier-Johnson configuration [3]. The sensor weights 16 kg and the power consumption averages 22 W. The DFMS is a high resolution mass spectrometer with a large dynamic range and good sensitivity. It covers a mass range of 12-140 amu/e and has a mass resolution of $m/\Delta m > 3000$ at the 1% peak height which corresponds to > 7000 at the 50% level. This allows separation of, e.g., ^{13}C and ^{12}CH. With an integration time of typically one second the recording of a whole mass spectrum measured with the Channel Electron Multiplier (CEM) detector from 12 to 140 amu/e takes approximately two hours. The mass resolution of the DFMS is high enough to measure interesting isotopic ratios of, e.g., the two nitrogen isotopes ($^{14}N^+$, $^{15}N^+$). This is of great importance in order to determine and explain the anomalous nitrogen isotopic ratios in comets.

RTOF. The RTOF is characterized by an extended mass range from 1 up to > 300 amu/e in order to identify organic material, e.g., polyaromatic hydrocarbons. The sensor weights 15 kg and consumes about 30 W. The high sensitivity of the RTOF sensor is essential with respect to the pressure range that is expected when Churyumov-Gerasimenko is at 3 AU where measurements are activated. The expected water production rates at perihelion, during peak activity, and at 3 AU at comet Churyumov-Gerasimenko are given in table 1.

Tab. 1: Expected water production rate and the corresponding pressure at 2 km from the nucleus for comet Churyumov-Gerasimenko [4].

Heliocentric distance	$Q(H_2O)$ [s^{-1}]	H_2O density [cm^{-3}] @ 2 km	Pressure [mbar]
Perihelion (1.3 AU)	4.1×10^{27}	2.0×10^{11}	6.0×10^{-6}
Peak activity	1.0×10^{28}	8.0×10^{11}	2.5×10^{-5}
3 AU	1.0×10^{23}	1.0×10^{7}	1.0×10^{-10}

An advantage of the RTOF sensor is that a full mass spectrum of the entire mass range (1-300 amu/e) that is only limited by the signal accumulation memory is recorded within 100 µs. The mass resolution in the triple reflection mode is $m/\Delta m > 4500$ at the 50% peak height. DFMS and RTOF complement one another.

COPS. The COPS weights 1.7 kg and consumes 7 W. It consists of two ionization gauges to determine the gas dynamics of the comet. One gauge is a nude hot filament extractor type Bayard Alpert ionization gauge [5]. It measures the total particle density with a nitrogen sensitivity of about 20 $mbar^{-1}$ at 100 µA. The other gauge, a closed ionization gauge, with its opening facing towards the comet, measures the molecular flow from the comet. Combining the results from both gauges and the known spacecraft orientation relative to the nucleus of the comet, the velocity and the density of the cometary gas can be calculated. In addition, this sensor serves as a safety instrument for Rosetta in case of pressure increases.

Anticipated Analyses: During the increasing activity of the comet from aphelion to perihelion more and more cometary material like dust particles as well as ice will evaporate. The evaporation products can easily be measured by the ROSINA mass spectrometers. Together with other instruments onboard Rosetta that are specialized on dust measurements it will be possible to determine the dust composition due to the capability of ROSINA to measure in an extended mass range (> 300 amu/e) with a high sensitivity and a large dynamic range. Therefore, the two ROSINA mass spectrometers support the dust analyses performed by the dust specialized instruments.

Conclusions: The ROSINA instrument package was designed to measure relevant elemental, isotopic, and molecular abundances from the onset of activity through perihelion. It will easily cope with the activity of Churyumov-Gerasimenko at 4 AU as well as at perihelion. Finally, it will analyze the composition of the volatile material over a large mass range with a large dynamic range, and it will significantly contribute to our understanding of the dynamics of this comet.

References: [1] Balsiger H. et al. (2001) *ESA SP-1165*. [2] Mattauch J. and Herzog R. (1934) *Z. Physik, 89,* 786. [3] Johnson E. G. and Nier A. O. (1953) *Phys. Rev., 91,* 10-17. [4] Schleicher D. G. and Millis R. L. (2003) DPS 35th Meeting, oral presentation, 30.06. [5] Redhead R. A. (1966) *J. Vac. Sci. Technol., 13,* 173-180.

METEOR SHOWERS FROM BROKEN COMETS. P. Jenniskens, SETI Institute (515 N. Whisman Rd., Mountain View, CA 94043; pjenniskens@mail.arc.nasa.gov).

Introduction: When Whipple [1] discovered a mechanism to accelerate meteoroids by the drag of water vapor in1951, the old idea of meteor showers originating from comet breakup went into remission. Even though comets were frequently observed to break, there was no strong evidence that the meteoroids generated in these discrete and relatively rare events accounted for our meteor showers on Earth. Now, recent minor planet discoveries have recovered remnants of those breakups in some of our strongest showers.

The giant comet hypothesis: Active Jupiter Family Comets are known to frequently break and shed a series of 10-m to 1000-m sized fragments [2]. Examples are the 1832 breakup of 3D/Biela and the 1995 breakup of 73P/Schwassmann-Wachmann 3. Both comets used to, or will in the future, pass by Earth orbit. During those fragmentations, meteoroids are created that can lead to temporary meteor showers on Earth when the resulting dust trails are steered in Earth path. If the amount of dust is substantial, fragmentations can even lead to annual showers when the streams evolve into elongated structures that cross Earth's path.

The idea that the fragmentation of comets is a source of meteoroids causing meteor showers on Earth was first proposed following the 1872 and 1885 Andromedid storms, which followed the breakup of lost comet 3D/Biela in 1832, and the continued fragmentation of the comet observed in the returns of 1846 and 1852 [3]. At the time, comets were seen by many as a flying sand bank, dust grains orbiting each other and held together by their mutual gravity [4] and there was no clear distinction between a comet ensemble and individual meteoroids.

In recent years, the products of fragmentations are known to be comets in their own right, possibly creating new meteoroid streams by water vapor drag. Nuclear fragments in orbits with other orbital period than the parent comet were implicated in the periodic returns of the Lyrids [5], which we now know are due to periodic perturbations by Jupiter, which steer a continuous trail of dust in Earth's path instead. Another example of comet fragmentation implicated as the source of a meteor shower is the Giant Comet Hypothesis for the origin of the Taurid complex [6]. While in my opinion the Taurid shower is indeed likely the product of comet fragmentation, most of the implicated minor bodies have been proven to be unrelated asteroids, instead.

Fragments of broken comets in meteoroid streams: In 1983, Fred Whipple discovered a minor planet 3200 Phaethon among the meteoroid stream responsible for the Geminid shower [7]. The reflectance properties of the minor planet (taxonomic type B) make the nature of this object as an extinct comet nucleus uncertain, but only because of the small perihelion distance. The surface of the minor planet and the properties of the meteoroids are altered from repetitive heating by the Sun. It has since been shown that the Geminids appear to have been created close to perihelion, more typical of comet ejection than asteroidal collisions [8].

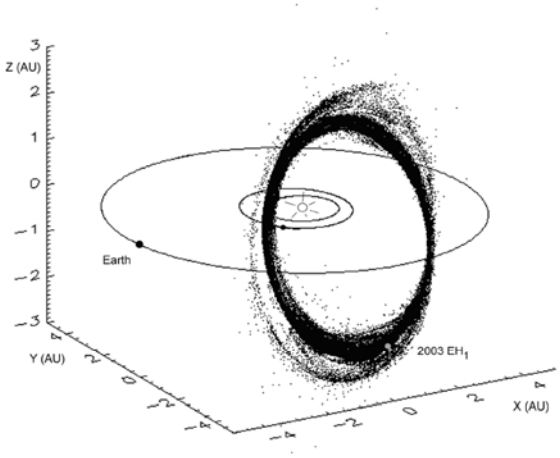

Fig. 1: 2003 EH_1 and the Quadrantid meteoroid stream, in a model by Jerémié Vaubaillon.

In 2003, I identified a minor planet 2003 EH_1 in the high-inclination orbit of the Quadrantids [9]. This is a massive stream, containing a thousand times more mass than typically ejected by an active Jupiter Family Comet. The minor planet passes outside of Earth orbit, but the stream evolves rapidly due to perturbations of Jupiter at aphelion (and at the ascending node). Accurate measurements of meteoroid orbits imply that the stream is not older than 500 years and must have formed in a short period of time. The comet C/1490 Y_1, seen in early 1491, may have been the manifestation of that breakup [10].

Now, a second such minor planet has been recognized, 2003 WY_{25}, which traces back to comet D/1819 W1 (Blanpain) [11]. The comet orbit is not known well and the comet was lost after the 1819 sighting,. However, 2003 WY_{25} has angular elements

within 0.2º from those of Blanpain at that time, and is therefore most likely a fragment of a breakup that must have occurred in the 18th or early 19th century, most likely just before the return of 1819.

We demonstrated that the dust generated in a breakup in 1819 would have wandered in Earth's path in 1951 and 1956, and could have been responsible for the strong 1956 Phoenicid outburst. The trail has not been in Earth's path since (at least not when Earth was at the node). Hence, the 1956 Phoenicids were likely the debris from the breakup of comet Blanpain in or shortly before 1819 [11].

More recently, the Marsden group of sunskirting comets was found to have a short orbital period [12], which implies that whatever was responsible for this large family of comet fragments is also responsible for the Daytime Arietids. The associated delta-Aquariids are then also formed after the breakup of a comet of that same group, albeit further evolved along a Kozai cycle.

In summary, the meteor showers that are likely from the fragmentation of comets rather than from Whipple-type ejection by water vapor drag are the Quadrantids, Daytime Arietids, delta-Aquariids, Andromedids, Phoenicids, and Geminids, and probably also the Capricornids, kappa-Cygnids, and Taurids, representing most of our annual showers.

Comet fragmentation: One of the more interesting results from comparing mass estimates of the comet fragments and the meteoroid streams of these Jupiter-Family-Comet parents is that the streams represent a mass no more than that of a single fragment [11]. In contrast, the disruption of long-period comet C/1999 S4 (Linear) was thought to have created as much as 200 times more mass than the sum of fragments combined [13]. Hence, the fragmentations in question are not necessary wholescale, but could pertain to the release of just a small number of cometesimals from their parent comet, in the process brightening the comet by a few magnitudes from the release of fine dust and gas.

The cause of those fragmentations remains unknown, but the impact of large meteoroids has been implicated as a mechanism to trigger such events [14]. While containing a relatively small amount of kinetic energy, such impacts may heat trapped subterranean gasses that can lead to sufficient pressure buildup to gently break off cometesimals.

The Deep Impact probe hit 9P/Tempel 1 in terrain dotted by impact craters that had clearly weathered similar events in the past. The approach images did not immediately show the breaking off of a fragment.

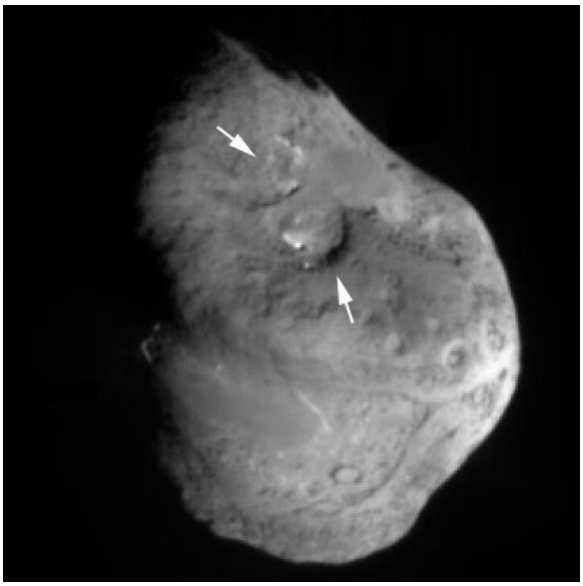

Fig. 2: Deep Impact target 9P/tempel-1. Arrows mark areas that might be the scars from recent fragmentation. Photo: NASA/JPL/Deep Impact.

However, the surface of comet 9P/Tempel 1 (Fig. 2) shows some areas with steep ridges that containing spots of high albedo terrain. Instead of impact craters, these structures could be the site of such fragmentation. In the case of 9P/Tempel 1, at least two 0.5-km sized fragments may have been lost from the comet. Other terrain is smooth, without much albedo variation, at the bottom of larger bowl-shaped depressions. That flat terrain likely resulted from dust fallen back to the comet that accumulated at the bottom of the bowls. It is not clear, at present, if that debris could have been created during the disruption, or was the result of normal Whipple-type ejection of meteoroids by the drag of water vapor instead.

References: [1] Whipple, F.L. (1951) *ApJ* 113, 464. [2] Sekanina, Z. (1997) AA 318, L5. [3] Olivier C.P. (1925) *Meteors*, Williams & Wilkins Co., Baltimore. [4] Lyttleton, R.A. (1948) MNRAS 108, 465. [5] Arter, T.R., Williams, I.P. (1995) *MNRAS* 277, 1087. [6] Clube, S.V.M., Napier, W.M. (1984) MNRAS 211, 953. [7] Whipple, F.L. (1983) IAUC 3881, 1. [8] Gustafson, B. Å. S. (1989) AA 225, 533. [9] Jenniskens, P. (2003) IAUC 8252 (Dec. 08). [10] Jenniskens, P. (2004) AJ 127, 3018. [11] Jenniskns, P., Lyytinen E. (2005) AJ (Sept., in press). [12] Marsden, B.G. (2004) MPEC 2004-X73. [13] Altenhoff, W.J., *et al.* (2002) AA 391, 353. [14] Babadzhanov, P.B., Wu, Z., Williams, I.P., Hughes, D.W. (1991) MNRAS 253, 69.

HYPERSEED MAC: AN AIRBORNE AND GROUND-BASED CAMPAIGN TO MONITOR THE STARDUST SAMPLE RETURN CAPSULE REENTRY ON 2006 JANUARY 15. P. Jenniskens,[1] P. Wercinski, M. Wright, J. Olejniczak, G. Raiche, D. Kontinos, and E Schilling,[2] G. Rossano and R.W. Russell, [3] M. Taylor, [4] H. Stenbaek-Nielsen, [5] G. Mcharg, [6] R. L. Spalding and K. Sandquist, [7] J. Hatton, [8] S. Abe,[9] R. Rairden, [10] D.O. ReVelle, [11] P. Gural, [12] D. Hladiuk and A. Hildebrand,[13] and F. Rietmeijer.[14] [1]SETI Institute (515 N. Whisman Rd., Mountain View, CA 94043; pjenniskens@mail.arc.nasa.gov), [2]NASA Ames Research Center, [3]The Aerospace Corporation, [4]Utah State University, [5]University of Alaska Fairbanks, [6]USAF Academy, [7]Sandia National Laboratories, [8]ESTEC/ESA, [9]Kobe University, [10]Lockheed Martin, [11]Los Alamos National Laboratories, [12]S.A.I.C., [13]University of Calgary, Canada. [14]University of New Mexico Albuquerque.

Introduction: The reentry of the Stardust Sample Return Capsule on 2006 January 16 is the fastest entry of a NASA space craft in NASA history and the first > 11 km/s since the Apollo era. The hypervelocity entry of a sample return capsule is an artificial meteor with flow conditions similar to natural asteroids for studies of the shock emissions and ablation process, without the confusion of fragmentation and the obscuring emissions from the ablated meteoric metals of natural fireballs. The entry is also a real-life test of key risk drivers for future Thermal Protection System (TPS) design: the amount of radiative heat flux and the response of the TPS.

Fig. 1: Genesis SRC entry.

Results from the Genesis SRC Entry campaign: The Stardust SRC entry follows the return of the Genesis SRC at the Utah Test and Training Range (U.T.T.R.) on September 8, 2004. That entry was observed in a first Hyperseed MAC mission, during which broadband optical emissions and infrasound signatures were detected. The anticipated emissions were calculated from a flow and radiation model, and were expected to be dominated by blackbody emission, but with measurable signatures from the shock wave [1]. The observations were only partially successful, because the spectrograph and imagers that needed to be aimed at the meteor did not acquire the object in the daytime sky due to a simple, yet significant, error in the instrument pointing simulation. Staring cameras did detect the bright SRC, as did ground-based infrasound detectors at Wendover and a handheld video camera. The results from the observations show that the surface-averaged brightness temperature was close to that predicted [2]. The infrasound signal was only a factor of two different from that calculated based on Apollo data [3].

The Stardust SRC entry: Stardust will be a night time reentry which permits intensified spotting cameras with a large field of view. The star background will provide a coordinate frame. We will now also have central access to the latest trajectory files from the Stardust mission navigators.

Stardust will enter Earth's atmosphere at a shallow angle of 8.2º, spin at 15 rates per minute, and experience a surface heat rate of about 1200 W/m^2. The peak deceleration in Earth's atmosphere will be 34 g. The phenolic impregnated carbon ablator (PICA) heat shield will bear the brunt of the entry.

The Genesis SRC was larger than the Stardust SRC (1.52m compared to 0.811m), but arrived at lower speed (11.0 km/s versus 12.9 km/s @ 135 km). Stardust's kinetic energy will be 1/4 that of Genesis, making the reentry 1.4 magnitudes fainter, but the higher speed will induce more intense shock emissions. Preliminary calculations show that the emission lines should stand significantly above the continuum emission from the hot surface area. The peak brightness (from a distance of 100 km) will be about -5 magnitude panchromatic and brighter at red and near-infrared wavelengths.

Hyperseed MAC: We will report on how results from the Genesis Hyperseed MAC mission help guide the ongoing efforts to bring together a second airborne mission using NASA's DC-8 Airborne Laboratory. This will enable a large team of researchers to view the entry above clouds and in a low-water-vapor line-of-sight. This airborne mission will be supported by ground-based observations.

References: [1] Jenniskens P., *et al.* (2005) *EMP (in press).* [2] Jenniskens P., *et al.* (1997) *AIAA Reno meeting. (submitted).* [3] ReVelle D.O., Edwards W., Sandoval T.D. (2005) *Met. & Planet. Sci. (in press).*

Additional Information: More information will be provided at the website http://reentry.arc.nasa.gov while the campaign unfolds.

DUST IN COMETS OBSERVED AT SUBMILLIMETER WAVELENGTHS

D. Jewitt[1], H. Matthews, S. Andrews
[1]Institute for Astronomy, University of Hawai'i, HI 96822; jewitt@hawaii.edu

The dust size distribution in comets is such that, while small particles dominate the scattering cross-section, it is the large particles which dominate the mass. Historically, most studies of cometary dust employed optical wavelength data and so were most sensitive to micron-sized particles in the cometary coma. This lead to dramatic under-estimates of the mass production rates in cometary dust and to unreasonably small values of the cometary dust/gas ratio.

The use of infrared and, more recently, submillimeter wavelength observations (Figure 1) has changed our appreciation of the number and role of large particles in comets. Large cometary particles are analogues of the dust sensed remotely from thermal excesses in the circumstellar disks of other stars: indeed, the cometary dust assemblage may be thought of as a frozen sample of dust from the Sun's own accretion disk. In this talk we will discuss the long-wavelength data available for comets, much of it acquired in a long-term program conducted at the James Clerk Maxwell Telescope. We will discuss implications for the mass loss rates and relate the cometary dust to precursor material in the accretion disk of the Sun.

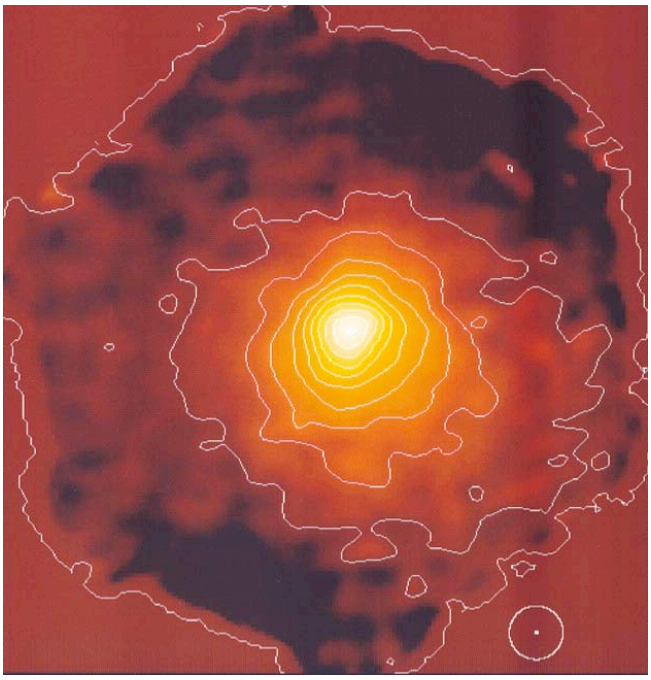

Figure 1

Image of C/Hale-Bopp taken at 850 μm with the SCUBA bolometer array. Field of view is 155" (160,000 km). The circle shows the 15" angular resolution of JCMT at this wavelength. Dust mass loss rate inferred from this image was near 1000 tonnes/second.

ORGANIC SYNTHESIS ON DUST: IMPLICATIONS FOR PROTOSTELLAR SYSTEMS. N. M. Johnson[1,2] and J. A. Nuth III[1]. [1]Astrochemistry Lab, NASA's Goddard Space Flight Center, Greenbelt, MD 20763 (njohnson@lepvax.gsfc.nasa.gov). [2]NAS/NRC Resident Research Associate.

Introduction: Hydrogen (H_2), nitrogen (N_2) and carbon monoxide are the most abundant molecular constituents in astrophysical environments, including protostellar nebulae. Although some organic molecules may be produced on very long timescales by the irradiation of ices formed on the cold surfaces of interstellar grains [1], pre-solar organics could be swamped by the efficient conversion of nebular H_2, N_2 and CO to simple organic materials. We carried out experiments that demonstrate that almost any surface can serve as a 'mediator' for this conversion process.

Surface-Mediated Chemistry: While it is unknown what exact process or combination of processes produced organics that are found in meteorites or are detected in comets and nebulas, one particular method that forms organics are Fischer-Tropsch type (FTT) reactions. Fischer-Tropsch type synthesis produces complex hydrocarbons by hydrogenating carbon monoxide via surface mediated reactions. The products of these reactions have been well-studied using 'natural' catalysts [2] and calculations of the efficiency of FTT synthesis in the Solar Nebula suggest that these types of reactions could make significant contributions to the composition of material near three AU [3]. We use FTT synthesis to coat Fe-silicate and Mg-silicate amorphous grains with organic material to simulate the chemistry in the early Solar Nebula. These coatings were found to be composed of macromolecular organic phases [4]. Previous work also showed that as the grains became coated, Haber-Bosch type reactions took place resulting in nitrogen-bearing organics [5].

We discuss the differences/similarities of the produced organics (solid and gas phase) and their production rates using either amorphous Mg- silicate grains or amorphous Fe- silicate grains as the starting material.

Experiments: We circulate CO, N_2, and H_2 gas through Fe- or Mg- amorphous silicate grains that are maintained at a specific temperature. The gases are passed through an FTIR spectrometer and are measured to monitor the reaction progress. Each cycle begins with 75 torr N_2, 75 torr CO, and 550 torr H_2 before the grains are brought to temperature (i.e., 400 or 500°C). After the gas has circulated for a predetermined amount of time, the heating element is turned off and the gas is pumped away. We repeat this process approximately fifteen times.

In addition to real time gas measurements using FTIR, we periodically collect a gas sample for additional analysis using a cold trap and a solvent (e.g., high purity acetonitrile). We analyze the 'trapped' gas sample using GCMS. Solid samples are analyzed using FTIR, GCMS (including pyrolysis) and potentially by NMR spectroscopy. Extraction techniques are also used to analyze the organic coatings.

Discussion: These experiments show that these types of reactions are an effective process to produce complex hydrocarbons. In the future, we will subject the reacted samples to thermal annealing and/or hydration to determine how these processes affect the deposited organic layers. These secondary processes would mimic what may have occurred on meteorite parent bodies and ideally give insight into the history of meteoritic organics. Overall, organics generated in this manner could represent the carbonaceous material incorporated in comets and meteorites.

Dust grains falling into a protostellar system would provide the surfaces that promote the reaction of H_2, N_2 and CO into both volatile organics and a macromolecular coating that continues to promote the formation of organic materials. Although the reaction is most efficient in the innermost regions of the nebula this does not pose significant problems as the reaction products as well as the coated grains can migrate back out to the far reaches of the nebula, thus seeding the entire nebula with the organic building blocks of life.

Acknowledgements: We thank M. Martin, J. Dworkin, G. Cody, and C. Alexander for their support.

References: [1] Gerakines, P. A. et al. 2004 *Icarus* 170:202-213. [2] Hayatsu R. and Anders E. 1981. *Topics in Current Chemistry* 99:1-37. [3] Kress M. E. and Tielens A. G. G. M. 2001. *Meteoritics & Planetary Science* 36:75-91. [4] Johnson N. M. et al. 2004. Abstract #1876. 35th Lunar & Planetary Science Conference. [5] Hill H. G. M and Nuth J. A. 2003. *Astrobiology* 3:291-304.

CRYSTALLINE SILICATE FORMATION AND COMETS. N. M. Johnson[1,2] and J. A. Nuth III[1]. [1]Astrochemistry Lab, NASA-Goddard Space Flight Center, Greenbelt, MD 20763 (njohnson@lepvax.gsfc.nasa.gov). [2]NAS/NRC Resident Research Associate.

Introduction: A traditional view of the early solar nebula and planet formation involves the outer edges being cold and wet and the interior regions remaining hot and dry. While this generalization is a gross over-simplification, it does give a nutshell idea of the early solar nebula. However, the problem with this view is that as more data is acquired, this simple model is no longer sufficient to explain all the observations. We focus on the existence of crystalline silicates in comets [e.g., 1,2]. In the traditional view, comets form by accumulating materials that formed at low temperatures and are stable in the 'comet-feeding-zone' at the outer edges. Such a zone would include gases and a variety of ices but not crystalline silicates. Crystalline silicates must form in the presence of high temperature and/or energy from shocks. There are a couple of places where these conditions could be met: the hotter, denser inner solar nebula or by shocks [3]. These two conditions are not mutually exclusive. Nuth [4] previously contended that amorphous silicates were annealed within the inner regions of the Solar Nebula and were later transported out beyond the snowline via nebular winds and ultimately incorporated into comets. This idea of outward transport is not without merit as Boss [5] shows that materials could move both inward and outward in the nebula. Others have also argued that outward transport is viable [e.g., 6]. Chondrules and CAIs have been proposed to form in the hottest inner regions of the nebula. If there was indeed outward migration, the Stardust mission will give direct evidence of this outward movement if it collects samples containing CAIs, for example. Shocks in the outer nebula can also anneal amorphous grains, and probably do, but the question is, "Can we determine if there is a dominant process or can either process be ruled out?"

We suggest that there is a direct and definitive observational test to distinguish between the relative importance of the two models for the origin of crystalline grains in comets: namely the presence or absence of crystalline iron-bearing silicates in the cometary grain population. This argument is presented in more detail in Nuth and Johnson [7] and in our poster at this workshop.

References: [1] Crovisier J. et al. (1997) *Science, 275,* 1904-1907. [2] Wooden, D. H. et al. (2004) *ApJ,* 612, L77-L80. [3] Harker, D. E. and Desch, S. J. (2002) *ApJ,* 565, L109-L112. [4] Nuth, J. A. (1999) *LPSCXXX*, 1726. [5] Boss, A. P. (2004) *ApJ*, 616, 1265-1277. [6] Prinn, R. G. (1990) *ApJ,* 348, 725-729. [7] Nuth, J. A. and Johnson, N. M. (2005) *Icarus*, submitted.

Thoughts on Small Body Exploration History and Prospects

T. V. Johnson
Jet Propulsion Laboratory, California Institute of Technology, Pasadena, CA 91109

Developing a viable program of small body (comets, asteroids, dust) space exploration has been difficult. The project landscape of the last thirty years or so is littered with the remains of proposed small body missions which never made it to the budget phase or were canceled (from Halley-Temple 2 to CRAF). The only early major successes were the ESA Giotto mission and the Soviet Vega missions, dedicated to Halley flybys. Following the Halley missions the NASA space science program had many proposals for small body missions of varying degrees of ambition but had little success in selling a major thrust in small body exploration, despite numerous advisory committee recommendations. Major progress in small body exploration has come about primarily by shifting the focus from large, dedicated missions to an approach combining use of existing assets (e.g. Galileo, Cassini), the Discovery mission line, and technology development through the New Millennium program. The result has been a greatly increased level of knowledge about these intriguing classes of objects and their environments: Galileo flybys of Gaspra and Ida (plus Dactyl), interplanetary dust observations on Galileo, ESA's Ulysses, and Cassini, the NEAR mission to Eros (flyby of Mathilde), DS1's encounter with Borrelly (plus demonstration of ion drive), the Stardust encounter with Wild 2 and upcoming sample return, the selection of DAWN to study main belt asteroids Vesta and Ceres, and the recent spectacular Deep Impact success. ESA has also pursued the major, cornerstone approach with the launch of Rosetta. What of the future? Continued use of the current strategy will undoubtedly increase our sampling and knowledge of small bodies, but the very success of the last two decades has resulted in the community's development of science objectives for the future (most recently through the NRC's decadal survey) which may only be achievable with larger more complex and costly missions, including sample return. This work was done at the Jet Propulsion Laboratory, California Institute of Technology under a contract from NASA.

Mineralogy and Densities of Cometary and Asteroidal IDPs Collected in the Stratosphere. [1]D. J. Joswiak, [1]D E. Brownlee, [2]R. O. Pepin and [2]D.J. Schlutter. [1]Dept. of Astronomy, 351580, University of Washington, Seattle, WA 98195, [2]Dept. of Physics, University of Minnesota, Minneapolis, MN 55455. e-mail: joswiak@astro.washington.edu

Introduction: IDPs collected in the stratosphere comprise astromaterials from both cometary and asteroidal sources [1]. Of primary interest are cometary IDPs as these particles are the only physical samples of comets available for study in the laboratory. IR spectroscopic measurements of comets taken during spacecraft flybys along with laboratory analyses of anhydrous IDPs indicate that comets are composed of complex mixtures of unequilibrated crystalline and noncrystalline materials including Fe-Mg-rich silicates, glasses, Fe sulfides, and organic compounds [2]. Since comets were formed at heliocentric distances of 5 – 50 AU in the solar nebula, these materials likely represent the first building blocks during solar system formation.

In a collaboration with the University of Minnesota, we have been conducting an ongoing investigation to determine which subset of IDPs collected from the stratosphere are likely to have originated from comets vs asteroids. We have compiled a database containing mass, density, ^{4}He abundance, atmospheric entry temperature, atmospheric entry velocity and mineralogy for IDPs that have likely cometary or asteroidal origins. Here we report on some of the results we have obtained on 32 stratospheric IDPs with an emphasis on the cometary IDPs.

Analytical Methods: Thirty two chondritic stratospheric IDPs ranging in size from 5 – 15 μm were systematically processed after removal and washing from six collector flags. Mass, density and bulk composition were measured for each IDP in the Cosmic Dust Lab at the University of Washington [3]. The particles were then embedded in either epoxy resin or sulfur and microtomed for mineralogical studies by TEM. Peak heating temperatures were measured at the University of Minnesota from the remaining particle in the potted butt by generating a stepped-He release curve [4]. The mineralogy of each IDP was obtained by detailed TEM/STEM/EDX investigations on microtomed sections using microanalytical EDX, SAED and high resolution imaging techniques.

Atmospheric Entry Velocities: The likely cometary or asteroidal origin for each IDP was determined using the temperature measured after 50% release of He with the atmospheric entry model of Love and Brownlee [5]. For the 32 IDPs measured, peak heating temperatures ranged from 505 – 1067 °C (Fig 1). Atmospheric entry velocities varied from 10.1 km/s to greater than 26 km/s (Fig 2). The IDPs were subdivided into low ($V \leq 14$ km/s), intermediate (14 km/s < $V < 18$ km/s) and high ($V \geq 18$ km/s) velocity groups. We believe that IDPs that fall in the low velocity group are likely have an asteroidal origin while those in the high velocity group are likely to have a cometary origin; we do not attempt to classify those in the intermediate velocity group.

Cometary IDPs ($V \geq 18$ km/s): Twelve IDPs have velocities consistent with a cometary origin (Fig 2); atmospheric entry temperatures range from 721 – 1016 °C. Measured densities range from 0.62 – 1.73 g/cm^3 with an average density of 1.03 g/cm^3 (Fig 3). Both non-crystalline and crystalline silicates including Mg-rich olivines, pyroxenes (enstatite, pigeonite, augite and diopside) and GEMS were observed in these IDPs (Table 1); grain sizes are typically 100 – 200 nm. Pyrrhotite, pentlandite, Fe-Mg-Al silicate glass (not GEMS), noncrystalline carbon, FeNi metal and occasional spinel and feldspar were also found. One IDP (U2070A-10A) with an entry speed of 20.3 km/s contained the hydrated minerals cronstedtite and saponite as major phases. A small amount of nearly pure forsterite was observed in this IDP as well.

Asteroidal IDPs ($V \leq 14$ km/s): Figure 2 shows that 4 of the 32 measured IDPs fall in the low velocity group. Atmospheric entry heating temperatures range from 505 – 1067 °C while IDP densities vary from 1.54 – 4.2 g/cm^3 with an average density of 3.3 g/cm^3(Figs 1 and 3). Three of the four IDPs are composed of the phyllosilicate minerals cronstedtite or saponite (Table 1). These minerals are generally poorly crystallized (this may be due to decomposition from atmospheric entry heating). Consistent chemical composition along with 0.71 nm or 1.0 – 1.4 nm lattice fringes were occasionally observed to confirm these phases. All contain minor quantities of pyroxenes. One IDP is phyllosilicate-free and composed of a mixture of grains typical of the cometary group – olivine, pyroxene and possibly GEMS. Pyrrhotite, pentlandite and Fe-Mg-Al silicate glass are also present in the asteroidal IDPs.

Discussion and Summary: Atmospheric entry velocities measured from 32 stratospheric IDPs indicate that 12 are probably comet dust while four likely have an asteroidal origin. Sixteen IDPs with intermediate velocities may have been derived from either source. Significant differences in density and mineralogy are evident between the cometary and asteroidal groups. The cometary IDPs have an average density of 1.03 g/cm^3 compared to 3.3 g/cm^3 for the asteroidal group. Mineralogically, the cometary IDPs do not contain phyllosilicate minerals (with one exception) but are composed of Mg-rich olivines, pyroxenes and glass, similar to materials observed by IR spectroscopic measurements taken by spacecraft from comets in the inner solar system [2]. Nearly identical mineralogy - crystalline Fo_{90}, crystalline clino+ortho pyroxenes (Mg/Fe+Mg≥0.9) amorphous olivine (Mg/Fe+Mg=0.5) and amorphous pyroxene (Mg/Fe+Mg=1.0) – was shown to comprise the best fit components to ISO SWS IR spectra taken from the ESA spacecraft of comet Hale-Bopp [6]. Hydrated

silicates could also be present at the 1% level or less. The minerals we observe in cometary IDPs are strikingly similar to those observed in comets.

References: [1] Joswiak, D.J., Brownlee, D. E., Pepin, R. O, and Schlutter, D.J., *LPSC XXXI*, 2000. [2] Hanner, M. S., in *Astromineralogy*, T.K. Henning ed., 171-188, 2003.. [3] Love, S. G., Joswiak, D. J. and Brownlee, D. E., *Icarus*, 111, 227-236, 1994. [4] Nier, A. O. and Schlutter, D. J., *Meteoritics* 28, 675-681, 1993. [5] Love, S. G. and Brownlee, D. E., *Icarus*, 89, 26-43, 1991. [6] Wooden, D. H. et al., *AJ*, 517, 1034-1058, 1 June 1999.

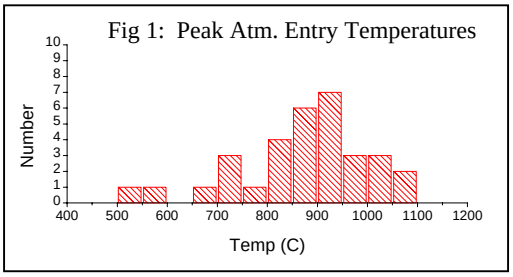

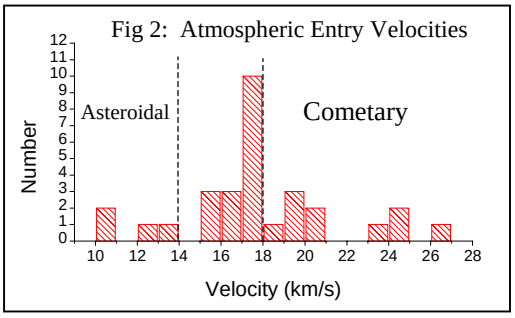

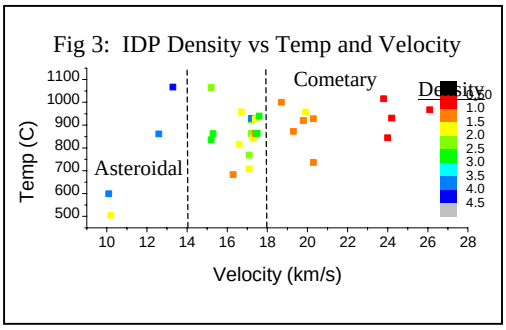

Figure Captions

Fig 1: Histogram showing measured atmospheric entry temperatures from 32 chondritic IDPs.

Fig 2: Histogram showing modeled atmospheric entry velocities from 32 choncritic IDPs. Four low speed IDPs ($V \leq 14$ km/s) are believed to have originated from asteroids while 12 high speed IDPs ($V \geq 18$ km/s) were likely derived from comets. Two IDPs with $V > 26$ km/s are not shown in the histogram.

Fig 3: IDP density as a function of atmospheric entry temperature and velocity. Cometary IDPs show lower overall density than asteroidal IDPs.

Table 1: Mineralogy in cometary and asteroidal IDPs

IDP	Vel (km/s)	Temp (°C)	Density (g/cm^3)	Olivine	Pyroxene	GEMS	Phyllo-silicates
			Cometary IDPs				
U2070A-4A	18.7	1000	1.29	$Fo_{80\text{-}84,\ 97}$	CEn_{99}, En_{99}, Aug	Yes	
U2012A-2G	19.3	872	1.13	$Fo_{88\text{-}93}$	En_{96}, Di?	Yes	
U2073B-8B	19.8	920	1.19	$Fo_{80\text{-}87,97}$	$En_{96\text{-}97}$	?	
U2-30C-4B	19.9	957	1.73				
U2012A-10G	20.3	736	1.00				
U2070A-10A	20.3	928	1.25	Fo_{99+}			Cron,Sap
U2073A-9A	23.8	1016	0.98	$Fo_{72\text{-}80,90}$	En_{93}, Ca-Px	?	
U2073A-7F	24.0	844	0.62	$Fo_{81\text{-}87,98}$	$En_{92,97}$; Pig	Yes?	
U2073B-2I	24.2	931	0.86	Fo_{95}	$En_{94,99}$; Aug, Pig	Yes	
U2073B-3C	26.1	967	0.88	Fo_{88}	CEn_{86}, Di, Pig	Yes	
U2012A-4J	>26	721	0.78				
U2073B-3A	>26	1009	0.70	$Fo_{77\text{-}78,\ 91}$	$En_{87,97}$; Di, Pig	Yes	
			Asteroidal IDPs				
U2012A-1G	10.1	599	3.68		Di		Sap?
U2012A-3G	10.2	505	1.54	$Fo_{65\text{-}67,87\text{-}97}$	En_{94}, Pig	Yes?	
U2012C-1B	12.6	861	3.64		En_{87}		Sap
U2073A-9F	13.3	1067	4.20	$Fo_{60\text{-}62}$	Aug		Cron?

Table 1: Entry velocities, measured stepped ^{4}He release temperatures, densities and partial mineralogy from cometary and asteroidal IDPs. Fo=forsterite, En=enstatite, CEn=clinoenstatite, Pig=pigeonite, Aug=augite, Di=diopside, Ca-Px=Ca pyroxene, Sap=saponite, Cron=cronstedtite.

THE E RING OF SATURN: MODELS VERSUS OBSERVATIONS. A. Juhasz[1] and M. Horanyi[2], [1]KFKI Research Institute for Particle and Nuclear Physics, Department of Space Physics, Budapest, Hungary, (juhasz@rmki.kfki.hu), [2]LASP University of Colorado, Boulder, Colorado, USA (Mihaly.Horanyi@colorado.edu).

A number of remote sensing and in situ observations of Saturn's E ring exist, including ground based and HST images taken during ring plane crossings, indirect observations of dust impacts measured by Voyager 1 and Pioneer 11 spacecraft, and the recent direct dust flux measurements by CDA onboard Cassini.

In this presentation we compare these observations with theoretical models that were developed to explain the dynamics and distribution of dust particles in the E ring [1,2,3,4,5,6,7].

Our earlier model [6] reproduced most remote sensing observations, including the color and the spatial distribution of the measured optical depth as function of distance from Saturn. We are now using a new fully 3D version of this code to follow the seasonal variations in the E ring [7], that is no longer assumed to remain azimuthally symmetric. We will report on the comparisons of the calculated in situ dust flux measurements with the CDA observations. Though the orbit-by-orbit comparisons remain difficult, the emerging global picture - based on multiple ring-plane crossings - can be used to adjust our model to optimize its predictive capability.

References: [1] Horanyi et al. (1992) *Icarus, 97*, 248-259. [2] Hamilton D.P. (1993) *Icarus, 101*, 244-264. [3] Hamilton D.P. and Burns J.A. (1994) *Science, 264*, 550-553. [4] Dikarev V.V. and Krivov A.V. (1998) *Solar System Research, 32*, 128-143. [5] Dikarev V.V. (1999) *Astron. Astrophys. 346*, 1011-1019. [6] Juhasz A. and Horanyi M. (2002) *JGR, 107*, 10.1029/2001JA000182. [7] Juhasz A. and Horanyi M. (2004) *GRL, 31*, L19703, 10.1029/2004GL020999.

THE EFFECT OF INTER-PARTICLE COLLISIONS ON THE DYNAMICAL EVOLUTION OF ASTEROIDAL DUST AND THE STRUCTURE OF THE ZODIACAL CLOUD. T. J. J. Kehoe[1] and S. F. Dermott[1], [1]Department of Astronomy, University of Florida, 211 Bryant Space Science Center, PO Box 112055, Gainesville, FL 32611-2055 (kehoe@astro.ufl.edu).

Introduction: Our approach to building detailed models of the zodiacal cloud is to utilize the results from numerical simulations of the dynamical behavior of its constituent dust particles. These dynamical models are then compared with observational data and refined.

Numerical Simulations: Due to computational constraints, our previous models of the zodiacal cloud [1] were limited to considering small particles, generally less than 100μm in diameter, that spiral rapidly into the Sun under the effect of Poynting-Robertson (P-R) drag [2]. Larger particles have correspondingly longer dynamical (i.e., P-R drag) lifetimes and hence require longer integration times. To enable a comprehensive numerical investigation of the orbital evolution of a realistic size distribution of particles in the zodiacal cloud has therefore required the application of a powerful new *N*-body code [3].

Moreover, we note that dust particles in the inner solar system with diameters of around 500μm have P-R drag lifetimes comparable to the timescale for the particle to be destroyed by inter-particle collisions [4], whereas the P-R drag lifetimes of particles much smaller than this are too short for them to be significantly affected by such collisions. To investigate the evolution of large dust particles has therefore required that, in addition to the previously modeled effects of radiation pressure, P-R drag, solar wind drag, and planetary perturbations, the effects of stochastic size changes due to particle fragmentation have also had to be incorporated into our numerical simulations of their orbital evolution. We have achieved this by employing a semi-analytic technique that combines the results of secular perturbation theory with numerical integrations using the *N*-body code discussed above.

Results: The orientation of the mean plane of symmetry of the zodiacal cloud is determined by the forced inclinations of the dust particles comprising the cloud together with their forced longitude of ascending nodes [5]. These forced elements are a function of semimajor axis, time, and the physical properties of the particles, such as size.

Figure 1 shows the forced inclinations as a function of semimajor axis for waves of 20-μm (green diamonds), 100-μm (red triangles), and 500-μm (blue squares) diameter dust particles. Each wave contained 1,000 particles that were released from the Veritas asteroid family at various epochs in the past so that they arrived at the semimajor axes indicated at the current epoch. The forced elements were calculated using the "particle on a circle" method [6]. Also shown (solid black line), is the forced inclination as a function of semimajor axis for a massless particle obtained using linear secular perturbation theory for the "zero-drag" case at the current epoch. The current inclination of Jupiter is shown as a dashed black line and the filled circle indicates the present location of the Veritas asteroid family. The figure clearly illustrates that as particle size increases, the forced inclinations of the dust particle waves tend towards the "zero-drag" secular solution, which is dominated by the effect of Jupiter in the region of the outer asteroid belt. Similar results were obtained in the case of the forced longitude of ascending nodes of the Veritas family particles, and for several other asteroidal sources investigated.

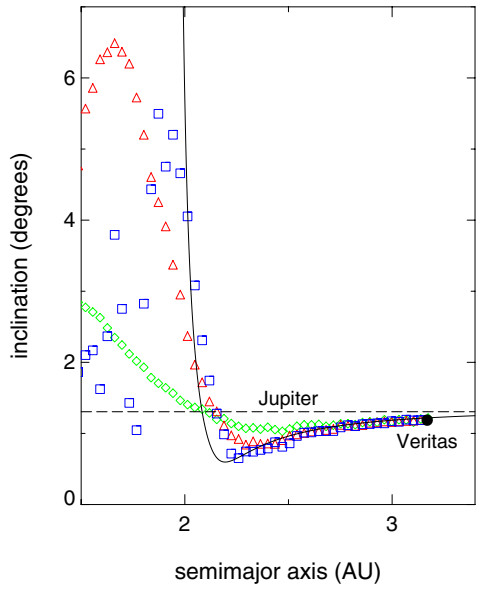

Figure 1

The forced inclinations as a function of semimajor axis for waves of 100-μm diameter dust particles are shown in Figure 2. These waves of particles were released from the Veritas asteroid family at various epochs in the past so that they arrived at the semimajor axes indicated when: (i) Jupiter's inclination was at its minimum value during its last secular oscillation (green diamonds), and (ii) at its maximum value (red triangles). The (i) green and (ii) red dashed lines indi-

cate the inclination of Jupiter at these two epochs. The solid black line again shows the forced inclination obtained using linear secular perturbation theory at the current epoch. The dotted and dashed black lines show the secular solution for a "zero-drag" massless particle when Jupiter's inclination was (i) at its minimum value and (ii) at its maximum value, respectively, during its last secular oscillation. At both these epochs, the forced inclinations of the dust particle waves continue to approximate the secular solutions, which are dominated by Jupiter in the outer asteroid belt.

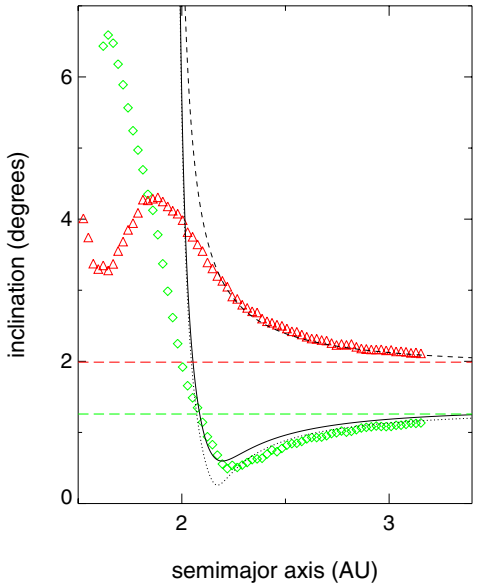

Figure 2

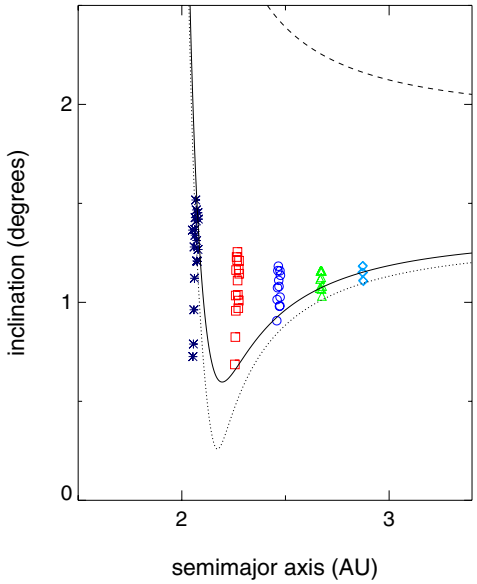

Figure 3

Figure 3 shows the forced inclinations as a function of semimajor axis for waves of collisionally evolved 20-μm diameter dust particles. The waves of particles were initially released as larger particles from the Veritas asteroid family 8.3Ma and fragmented at various epochs in the past so that they arrived at the semimajor axes indicated at the current epoch. The solid black line shows the forced inclination as a function of semimajor axis for a massless particle obtained using linear secular perturbation theory for the "zero-drag" case at the current epoch. The dotted and dashed black lines show the secular solution for a "zero-drag" massless particle when Jupiter's inclination was at its minimum value and its maximum value, respectively, during its last secular oscillation. The dispersion in the forced inclinations of the waves of 20-μm diameter particles at each semimajor axis arises because they were generated at different epochs in Jupiter's secular oscillation cycle.

Discussion: The orientation of the mean plane of symmetry of the zodiacal cloud outside 2AU is dominated by the effect of Jupiter as it evolves through its secular cycle. It is for this reason that we are able to observe the solar system dust bands discovered by IRAS [7]. The inner edge to the dust bands at 2AU results from the significant effect of secular resonances on particle orbits that disperses the dust band signal to the extent that it merges naturally into the flux from the background zodiacal cloud. The effect of interparticle collisions also introduces dispersion in the distribution of the forced elements of the particles as a result of the variation of Jupiter's orbital elements, and the "zero-drag" secular perturbation solution, over the course of a secular cycle. These new results contribute to a more accurate description of the orbital evolution of a realistic size distribution of zodiacal cloud particles and are now being employed to build detailed models of the solar system dust bands.

References: [1] Grogan K. et al. (2001) *Icarus, 152,* 251–267. [2] Wyatt S. P. Jr. and Whipple F. L. (1950) *ApJ, 111,* 134–141. [3] Kehoe T. J. J. et al. (2003) *AJ, 126,* 3108–3121. [4] Wyatt M. C. et al. (1999) *ApJ, 527,* 918–944. [5] Dermott S. F. et al. (2001) in *Interplanetary Dust,* edited by Grün E, Gustafson B. Å. S., Dermott S. F., and Fechtig H. [6] Dermott S. F. et al. (1992) in *Chaos, Resonance and Collective Dynamical Phenomena in the Solar System,* edited by Ferraz-Mello S. [7] Low F. J. et al. (1984) *ApJ, 278,* L19–L22.

Acknowledgments: This work was supported by NASA under Grant Nos. NAG5-11643 (PGG) and NAG5-13105 (ADP).

DUST PRODUCTION AND NUCLEUS EVOLUTION. H. U. Keller[1], Yu. V. Skorov[1,2], and G. N. Markelov[3], [1]Max-Planck-Institut für Sonnensystemforschung, 37191 Katlenburg-Lindau, Germany, [2]Keldysh Institute of Applied Mathematics, Miusskaya pl. 4, 125047 Moscow, Russia, [3]AOES, Haagse Schouwweg 6G, 2332 KG Leiden, The Netherlands.

Physical properties of comets like their density, porosity, and thermal conductivity are apparently determined by cometary evolution and history. These primordial differences affect the processes occurring when a comet is heated by the Sun. At the same time the release of volatiles influences the physical properties of the nucleus changing its porosity, e.g. forming a dust crust on the surface etc.

A complete physical description of the energy and mass transfer inside and outside the nucleus is a complicated problem. Due to the high porosity and the presence of transparent ice solar light can penetrate to a substantial depth leading to volume energy absorption in the uppermost porous layer of a cometary nucleus [1,2]. Note that the nucleus and the innermost coma of an active comet constitute a interacting physical system: both heat and mass are exchanged between the two regions, and their physical properties develop in close symbiosis. Therefore correct thermo physical modelling of a comet cannot be restricted to the nucleus itself - the whole system must be considered simultaneously [3,4]. This motivated us to a revision of the conventional model of a cometary nucleus. The following important aspects are now included: i) radiative energy transport in porous media; ii) energy transport by sublimation products; iii) heat and mass exchange between the nucleus and the innermost coma, iv) DSMC model of dust-gas flow in the innermost coma region [5].

We demonstrate that for a porous cometary nucleus vapour molecules escape from the non-isothermal upper sub-surface layer. High porosity leads to a significant decrease of the effective gas flux of volatiles and, as a result, the total dust production decreases. More of the absorbed energy is available to be transferred into the interior of the nucleus. The dependence of the gas production rate on the heliocentric distance is different for comets of different morphology of the uppermost surface layers (e.g. for the comets with surface or layer energy absorption). In the frame of kinetic DSMC model fields of density and velocity are calculated for the gas and for the dust. We show that the spatial structure of inner-most dust-gas coma is sensitive to the nucleus shape as well as to the variations of local gas production rates. In general, spatial structure of the innermost coma (both gas and dust) is a result of interactions of gas flows sublimated from different surface regions. We conclude that the nucleus shape as well as physical properties of nucleus play the major role in interpretation of innermost coma.

References:

[1] Skorov Yu. V. et al. (2001*) Icarus, 153*, 180. [2] Skorov Yu. V. et al. (2002) *Earth, Moon, and Planets, 90*, 293. [3] Davidsson B. J. R. and Skorov Yu. V. (2002) *Icarus, 56*, 223. [4] Davidsson B. J. R. and Skorov Yu. V. (2004) *Icarus, 168*, 163. [5] Skorov Yu. V., Markelov G. N., and Keller H. U. (2004) *Solar System Research, 38*, 455.

INTERACTION OF SATURNIAN DUST STREAMS WITH THE SOLAR WIND

S. Kempf[1], R. Srama[1], Mihaly Horányi[2], M. Burton[3], and E. Grün[1,4]

[1] MPI für Kernphysik, Saupfercheckweg 1, 69117 Heidelberg, Germany [2] Laboratory for Atmospheric and Space Physics, University of Colorado, Boulder, Colorado 80309, USA [3] Jet Propulsion Laboratory, Pasadena, California 91109, USA [4] Hawaii Institute of Geophysics and Planetology, University of Hawaii, 1680 East West Road, Honolulu 96822, USA

One of the major findings during the approach of the Cassini spacecraft to Saturn was the discovery of high velocity streams of nanometer-sized dust originating from the inner Saturnian system [4]. Until then, only the Jovian system was known to be a source of dust streams [1]. The dust stream phenomenon is of particular interest for a few reasons: (i) outside the planetary magnetosphere the stream particle dynamics is governed by the interaction with the solar wind plasma [2]; (ii) stream particles are the fastest solid bodies of the solar system known so far [6]; (iii) dust streams may transport material from areas which cannot be explored in-situ by space probes [4].

Numerical simulation by Zook et. al [6] proved that for the Jovian streams only grains of about 10 nm with speeds exceeding 200kms^{-1} reproduced the observations by Ulysses. Based on the impact signals caused by the Saturnian stream particles as well as by numerical simulations [3] those grains were found to have similar properties (radii ranging between 2 and 25 nm, speeds $\geq$ 100kms^{-1}). Furthermore, the simulations indicated that particles detected at large distances from Saturn most probably originated from the outskirts of Saturn's A ring. Surprisingly it was found that stream particles predominately consist of a silicon-bearing material[5] even though Saturn's rings are composed of water ice. This proposes that stream particles are rather the impurities of the icy ring material than the ring material themselves.

Here we report on results based on one year of continuous monitoring of Saturnian stream particles by the Cosmic Dust Analyser (CDA) on the Cassini spacecraft. All dust bursts detected within 150 Saturnian radii so far clearly coincided with the spacecraft's traversal through 'co-rotating interaction regions' (CIR) in the interplanetary magnetic field (IMF) – regions characterised by compressed plasma, increased solar wind speed, and enhanced magnetic field strength (Fig. 1). This finding together with our analysis demonstrates that the peculiar properties of dust streams can be explained by the interaction of the charged grains with the plasma inside the CIRs.

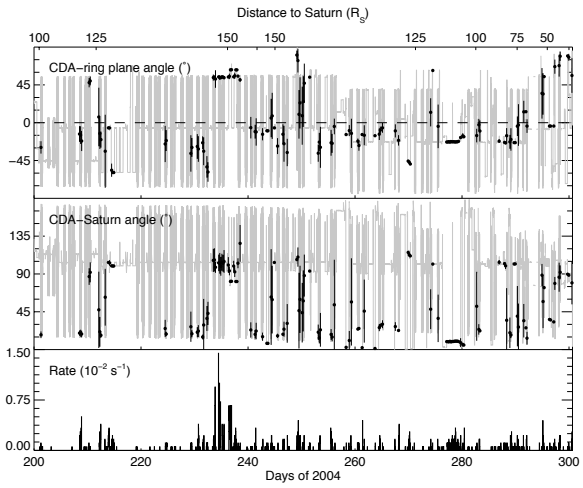

Figure 1: Impact rate and directionality of stream particles recorded during Cassini's first revolution around Saturn outside Titan's orbit spanning days 200 and 300 in 2004. The upper panel shows the angle between the CDA instrument normal and Saturn's ring plane, the middle panel indicates the angle between the CDA and the Cassini-Saturn line of sight. The mean angle is plotted whenever more than 2 impacts within 4 hours were registered; the attached bars indicate the 1-σ deviation from the mean angle. The gray solid line marks the evolution of the CDA normal due to the varying spacecraft orientation. The lowermost panel shows the stream particles impact rate. The pronounced impact bursts around day 210 and around day 235 of 2004 coincide with Cassini's traversal through co-rotating interaction regions in the solar wind. Note also that the directionality of the streams changed during these periods.

References

[1] E. Grün et al (1993) *Nature*, 362:428–430.
[2] D.P. Hamilton and J.A. Burns (1993) *Nature*, 364:695–699.
[3] S. Hsu and S. Kempf (2005) in prep.
[4] S. Kempf et al. (2005) *Nature*, 433:289–291.
[5] S. Kempf et al. (2005) *Science*, 307:1274–1276.
[6] H.A. Zook et al. (1996) *Science*, 274:1501–1503.

LUNAR SEISMIC DEVELOPMENT AND GAS-DUST STREAMS; GENESIS OF LIFE

Oleg B. Khavroshkin , Vladislav V. Tsyplakov,
Schmidt Institute of Physics of the Earth, RAS, B .Gruzinskay, 10,
Moscow, D-242, 123995 GSP-5 Russia, e-mail: khavole@ifz.ru

Review of Main Results of Lunar Seismic Development

Introduction: Results of previous research related to lunar seismicity (Nakamura Catalogue) and cosmogonic objects and processes are briefly outlined.

The Mapping of Impact Processes from Meteoroid Streams and Solar Wind on the Moon into Durations of Seismograms: Data of annual histograms (distributions) for durations of seismograms from exogenous acting on the Moon were analyzed. Peculiarities of these actions and their comparison with data of optic lunar events were taken into consideration. It has been found that dust-gas plasma of meteoroid streams and solar wind are modulated by Sun free oscillations. Histograms from meteoroid streams with intensity of 4-8 impact/days contain durations corresponding to periods of free lunar oscillations.

The Temporal Structure of Meteoroid Streams and Lunar Seismicity; the Peculiarities of Shape of Histogram Envelopes: The shapes of histogram envelopes for annual interval are changed from the Gauss curve to a more complicated one. It betokens the unsteady-state of seismic processes and, at times, their similarity to earthquake recurrence curves for regions of mines and/or to energy distribution for powerful solar bursts.

Simple Estimation for Non-gravity Effects on the Moon: Estimations of integral pressure on the Moon by solar wind (under undisturbed Sun and Sun burst) and gas-dust component of meteoroid streams have been made. Energy of these disturbances (under Sun bursts or its maximum stream density) is enough for initiation of free Moon oscillations and recording lunar seismic events.

Conclusions: The Moon is unique cosmogonic and astrophysical detector which can be realized by information of its own seismicity.

Manifestation of Gas-Dust Streams from Double Stars on Lunar Seismicity

Information content of the Nakamura`s Catalog of moonquakes is very rich: from solar-earth tides to clustering among the meteoroid streams [1,2]. The histograms from meteoroid-impact seismic data revealed the seismic wave responses of the Moon to solar oscillations and the action on the lunar surface by dust-gas plasma of meteoroid streams [3]. The time series of seismic events were generated as follows: on the ordinate axis the peak amplitudes of events in standard units, on abscissa axis - seismogram durations of the same moonquakes and subsequent time intervals between them were used [4]. Spectrum of the series of meteoroid streams disclosed time picks on orbital periods of some planets and their satellites and solar oscillations [4, 5]. The research of peculiarities of histogram envelopes [3] and comparative common analysis of solar bursts data and mass meteoroid distribution are confirmed [3, 4] and reveal Forbush`s effect for gas-dust plasma [6]. Hidden astrophysical periodicities of lunar seismicity were earlier obtained from analysis of time series [7] similar to series [4]. A part of results (picks) presents orbital periods of double stars nearest to the Solar system [7]. The path of results of [7] is presented in Table.

The first hypothesis for explanation of this result is existing gas-dust streams from binary stars near the solar system and their interaction with lunar surface; the second hypothesis is connected with the gravitation radiation from the same stars. Probably the first hypothesis is more real. First hypothesis for explanation of the Table results is existing gas-dust streams from binary stars near systems solar system and interacting with lunar surface; second is correlation them to the gravitational radiation from the same stars. We suppose that first hypothesis is more real.

Table

Characteristic of binary stars systems and picks of the lunar seismicity periodicity.

N Tabl 1	lunar periods, day	Name of system	Half period /period day	Masses of component solar unit.		distans parsec	Gravitation radiation. Gd/s
4	6.7	V380 Cyg	6.21	13.3	7.6	4168	10^{21}
		CV Vel	T=6.89	6.0	6.0	1047	
5	4.8	V356 Sgr	4.45	12.3	4.7	3090	10^{21}
6	3.5	CV Vel	3.44	6.0	6.0	1047	$2*10^{21}$
		h Aql	3.58			100	
7	2.25	UW Cma	2.20	43.5	32.5	8912	$5*10^{24}$
8	2.03	AG Per	T=2.029	4.5	4.5	660	
		α Vir	2.007	10.3	6.4	257	$3*10^{22}$
9	1.33	V906 Sco	1.393	3.5	2.8	251	
10	0.966	G Aql	0.975	6.8	5.4	549	$2*10^{23}$

11	0.666	Y Aql	0.651	7.5	6.9	275	$5*10^{23}$
12	0.543	IM Mon	0.595	8.4	5.6	724	$1*10^{24}$
14	0.323	VV U.Ma	0.343	2.1	0.5	512	$1*10^{22}$
		YY Eri	T=0.321	0.76	0.5	42	$1*10^{22}$
16	0.265	i Boo	0.268	1.35	0.68	12	$1*10^{23}$
20	0.160	SW Lac	0.160	0.97	0.82	74	$1*10^{23}$
21	0.142	j U.Mi	T=0.143			>100	
28	0.0751	j. U.Mi	0.0715				
29	0.0559	WZ Sge	T=0.0559	0.08	0.6	100	
34	0.0285	WZ Sge	0.0280	0.08	0.6	100	$4*10^{22}$

First hypothesis for explanation of the Table results is existing gas-dust streams from binary stars near systems solar system and interacting with lunar surface; second is correlation them to the gravitational radiation from the same stars. We suppose that first hypothesis is more real.

Genesis of Life

If the solar system is reached by the gas-dust streams from binary stars, then all bodes in space have particles of star dust on their surfaces and/or atmospheres. Solar system has made 8-10 revolutions around galactic center and thus captured dust from many thousands stars. As these stars caught in turn dust particles from other stars too then probably our solar system has mainly dust samples from all objects of our galaxy. The age of galaxy and old stars is approximately more than15 billion years and that of the Earth is only ~ 4,5 Gyr. Genesis of Life for the Earth has not more than 3 billion years. Thus comparative analysis of simple balance of these times shows that the genesis of Life for Earth is the result of galactic processes/objects and not of the solar system of course. After formation of the solar system all old and new captured dust particles are first accumulated in the Oort cloud and then they are carried by comets to planets. The modern state of the Earth exists for more than 3 billion years, so possibilities for appearing Life were always. These processes had happened a few times during this period of the Earth state. We must attach modern data of archaeology to confirm these results.

References

1. Sadeh D. Possible siderial period for the seismic lunar activity // Nature, 1972. Vol. 240, p.139
2. Oberst J. and Nakamura Y. A Search for Clustering among the Meteoroid Impacts Detected by the Apollo Lunar Seismic Network // ICARUS, Vol. 91, 315-325, 1991; Balazin M. and Zetzsche A. // PHYS.STAT.SOL., Vol.2, ,1962 1670-1674
3. Khavroshkin O.B. and Tsyplakov V.V. Meteoroid stream impacts on the Moon: Information of duration of the seismograms / In: Proceedings of the Conference METEOROID 2001, Swedish Institute of Space Physics, Kiruna, Sweden, 6-10 August 2001
4. Khavroshkin O.B. and Tsyplakov V.V., Temporal Structure of Meteoroid Streams and Lunar Seismicity according to Nakamura's Catalogue / In: Proceedings of the Conference METEOROID 2001, Swedish Institute of Space Physics, Kiruna, Sweden, 6-10 August 2001
5. O.B.Khavroshkin, V.V.Tsyplakov. Moon exogenous seismicity: meteoroid streams, micrometeorites and IDPs, Solar wind // Herald of the DGGGMS RAS: Electr. Sci.-Inf. J., 4(21)'2003
http://www.scgis.ru/russian/cp1251/h_dgggms/1-2003/scpub-3.pdf
6. O.B.Khavroshkin, V.V.Tsyplakov. Peculiarities of envelops of histograms of lunar impact seismogram durations / In: Geophysical research essays. Schmidt United Institute of Physics of the Earth Press, Moscow, 2003. 471 p., (in Russian).
M., ОИФЗ РАН, 2003, 471с.
7. O.B.Khavroshkin, V.V.Tsyplakov. Hidden astrophysical periodicities of lunar seismisity // Herald of the DGGGMS RAS: Electr. Sci.-Inf. J., 4(14)` 2000
http://www.scgis.ru/russian/cp1251/h_dgggms/4-2000/scpub-3.pdf

COSIMA: A High Resolution Time-of-Flight Secondary Ion Mass Spectrometer for Cometary Dust Particles on Its Way to Comet 67P/Churyumov-Gerasimenkov

J. Kissel[1], H. Höfner[2], G. Haerendel[2], S. Czempiel[2], J. Eibl[2], H. Henkel[3], A. Koch[3], A. Glasmachers[4], K. Torkar[5], F. Rüdenauer[6], W. Steiger[6], F. R. Krueger[7], E. K. Jessberger[8], T. Stephan[8], E. Grün[9], R. Thomas[10], Y. Langevin[11], H. von Hoerner[3], J. Silen[12], J. Rynö[12], M. Genzer[12], K. Hornung[13], R. Schulz[14] M. Hilchenbach[1], H. Fischer[1], H. Krüger[1], C. Tubiana[1], L. Thirkell[10], K. Varmuza[15] and the COSIMA team.

(1) MPI für Sonnensystemforschung, Max-Planck-Str. 2, D-37191 Katlenburg-Lindau; (2) MPI für extraterrestrische Physik, Giessenbachstr., D-85740 Garching; (3) von Hoerner und Sulger GmbH, Schlossplatz 8, D-68723 Schwetzingen (4) UNI/GH Wuppertal FB 13, Lehrstuhl f. Messtechnik, Fuhlrottstr. 10, D-42097 Wuppertal; (5) Inst. für Weltraumforschung, Infeldgasse 12, A-8010 Graz; (6) Inst. für Physik, Forschungszentrum Seibersdorf, A-2444 Seibersdorf; (7) Ingenieurbüro Krueger, Messeler Str. 24, D-64291 Darmstadt; (8) Inst. für Planetologie der Uni Münster, Wilhelm Klemm Str. 10, D-48149 Münster; (9) MPI für Kernphysik, Saupfercheckweg 1, D-69117 Heidelberg; (10) Laboratoire de Phys.& Chim. de L'Environment, 3 Av. De la Recherche, F-45071 Orléans; (11) Inst. D'Astrophysique, Bat.121, Faculté des Sciences d'Orsay, F-91405 Orsay; (12) Finnish Meteorological Inst., Department of Geophysics, Vuorikatu 15, SF-00101 Helsinki 101; (13) Universität der Bundeswehr LRT-7, Werner Heisenberg Weg 39, D-85577 Neubiberg; (14) ESA/ESTEC, NL-2200 AG Noordwijk; (15) Labor Chemometrie, Inst. für Verfahrenstechnik, Umwelttechnik und Techn. Biowissenschaften, TU Wien, A-1060 Wien

The **CO**metary **S**econdary **I**on **M**ass **A**nalyser (COSIMA) is a high-resolution time-of-flight (TOF) mass spectrometer system on board ESA's ROSETTA spacecraft flying to comet 67P/Churyumov-Gerasimenkov. COSIMA will collect cometary dust particles on metal black targets which are exposed to space. After target exposure dust particles with sizes $10\,\mu$m and bigger are identified on the target with an optical camera. An Indium ion beam is shot onto the particle surface and material from the particle is sputtered and ionised. The secondary ions are accelerated in an electric field and from the mass- and charge-dependent flight times of the ions a time-of-flight secondary ion mass spectrum (TOF-SIMS) is measured with a mass resolution of $m/\Delta m \approx 2000$ at $m = 100$. During commissioning in 2004 the COSIMA flight instrument performed according to specification. The first TOF-SIMS spectra in space in positive and negative ion modes were obtained from one of the instrument targets. COSIMA is now ready for the comet. The goal of the COSIMA investigation is the in-situ characterisation of the elemental, molecular, mineralogic and isotopic composition of dust particles in the coma of comet Churyumov-Gerasimenkov. Comets are remainders from the formation of the solar system and, therefore, analysis of cometary material can give important insights into the conditions of the first stages of planetary system formation and cometary evolution.

ANALYSIS OF COSMIC DUST BY THE 'COMETARY AND INTERSTELLAR DUST ANALYSER' (CIDA) ONBOARD THE STARDUST SPACECRAFT. J. Kissel[1], F. R. Krueger[2] and J. Silen[3], [1]Max-Planck-Institute for Aeronomy, D-37191 Katlenburg-Lindau, [2]Messeler Str. 24, D-64291 Darmstadt, [3]Finnish Meteorological Institute, Vuorikatu 24, SF-00101 Helsinki

The CIDA instrument on board the Stardust spacecraft is a time-of-flight mass spectrometer used to analyze ions formed when fast dust particles strike the instrument's target. The instrument has been calibrated with high speed dust particles at the Heidelberg dust accelerator. Laboratory work has been performed to better understand the ion formation processes of organic grains impacting at speeds of >15 km/s and to relate them to some other ion formation methods. On board Stardust spacecraft a series of positive and negative ion mass spectra from the impact of (apparently) interstellar and cometary dust particles has been collected since 1999. In the spectra of 45 presumably interstellar particles, quinone derivates were identified as constituents in the organic component. The 29 spectra obtained during the flyby of Comet 81P/Wild 2 on 2 January 2004 confirm the predominance of organic matter. In contrast to interstellar dust organic material in cometary dust seems to have lost most of its hydrogen and oxygen as water and carbon monoxide. These are now present in the comet as gas phases, whereas the dust is rich in nitrogen-containing species. Sulfur ions were detected in one spectrum, which suggests that sulfur species are important in cometary organics.

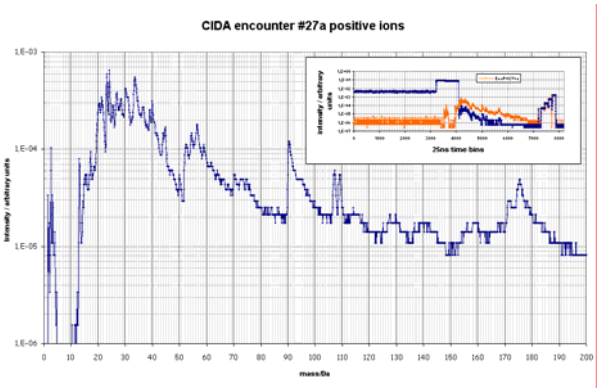

CIDA positive ion spectrum of a ~1 pg particle of mixed composition recorded during Wild 2 encounter. The spectrum is typical for nitrogen organic chemistry. The m/z = 107, 109 doublet is due to the Ag^+ from the target. The inset shows the raw data.

EXPERIMENTAL DETERMINATION OF THE RADIATION PRESSURE FORCES ON AN INDIVIDUAL DUST PARTICLE. O. Krauss and G. Wurm, Institute for Planetology, University of Münster, Wilhelm-Klemm-Str. 10, 48149 Münster, Germany, e-mail: okrauss@uni-muenster.de.

Introduction: As soon as the circumstellar disk of a forming planetary system gets optically thin submicron and micron-sized dust particles are subject to the radiation pressure of the central star. The influence of this force on the dust is then present throughout the further evolutionary stages of the system. Today, the dynamic evolution of cometary, asteroidal and also interstellar dust particles in the Solar System is influenced by the radiation pressure of the Sun [1].

The radiation pressure force is usually quantified by its ratio to the gravitational force of the star or the Sun, referred to as β. This value describes the balance between these two counteracting forces in radial direction. Radiation pressure can substantially reduce the lifetime of dust grains with high β values in the Solar System or a circumstellar disk. For spherical grains β usually reaches a maximum at particle sizes on the order of 100nm, depending on the dust material and on the properties of the star. For larger spheres β decreases rapidly.

However, the dust particles in a disk or in interplanetary space are, in general, irregularly shaped, they may have an aggregational structure or are more or less porous. The details of how these morphological features determine the radiation pressure experienced by a dust particle are not very well understood. Various calculations yield that fluffy aggregates do not show a strong decrease of β with increasing particle size [2, 3]. That means that 10µm aggregates of absorbing material can have a β value considerably larger than unity. The β values for non-spherical particles also become dependent on the orientation of the particle with respect to the incident radiation. Computational studies on spheroids [4] and cylinders [5] show a strong dependence of β on the orientation angle and the aspect ratio. Furthermore, irregularly shaped particles will have a radiation pressure force component that is perpendicular to the direction of irradiation, which is due to their asymmetrical light scattering. This transverse force component may reach several 10% of the radiation force in forward direction [4, 6, 7].

Experimental data on these features of radiation pressure that are related to the irregular shape or aggregational structure of dust particles is very rare.

Dynamic measurement of radiation pressure: We have developed a measurement technique that allows for measuring the radiation pressure forces on an isolated dust particle that is levitated in an electrodynamic trap [7, 8]. The particle is irradiated by an intense laser pulse, and its change in velocity is observed. During this process of measurement the electric fields of the trap are turned off, leaving the particle under free fall conditions without any external forces acting on it. By measuring the velocity difference of the particle and the energy density of the laser pulse the β value is obtained.

The effect is observed in two dimensions, which yields also the transverse component of the radiation pressure force. For a graphite aggregate as described below with a size of 17x7µm (largest x smallest extent) we measured a mean ratio of the transverse to the radial component of the radiation pressure force of 70% with a strong dependence on the orientation of the particle for each individual measurement [7].

Since the particle is recaptured by the trap after the measurement, a series of thousands of measurements can be performed with a single particle. Due to the wide tuning range of the applied laser source a radiation pressure spectroscopy from 220nm to 2500nm is possible.

Several techniques are currently being tested and implemented in order to charge an individual sample particle by UV or electron irradiation, put it into the trap, and retrieve it after the measurement non-destructively, which will make this method also applicable to IDP samples or particles obtained from sample return missions.

β values of graphite aggregates: First measurements applying the method described above were done with graphite aggregates in the 10µm size range. These particles consist of flake-like constituents of various sizes. The overall size of such an aggregate varies in different dimensions. Their most dominant morphological feature is that they are plates with a thickness of 100nm or less and a surface of several μm^2, which stick loosely together and are oriented in different directions. This results in a very high projected-area to mass ratio of these aggregates.

In the following we show data of about 600 measurements for a graphite aggregate of 17x6µm in size. In Fig 1 the obtained β values are plotted against the energy density of the laser pulse. Each data point is an average of 30 individual measurements using the same set of parameters.

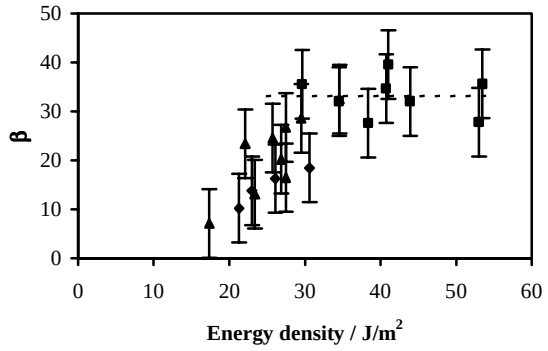

Fig 1. Measured β values as a function of laser pulse energy density for a 17x6µm graphite aggregate. The different symbols correspond to three different sets of measurements with the same particle performed on different days.

It can be seen that for energy densities larger than 30J/m^2 β reaches a constant value of about 33 (±4). Thus, above a certain threshold that is due to the experimental method the β value is independent of the laser energy density as expected. The rather high value of β is due to the typical structure of the graphite aggregates. Their large surface areas result in large cross sections for radiation pressure while at the same time the mass of these aggregates of loosely connected plates is very low.

In Fig 2 the β value of the same graphite particle is shown as a function of the wavelength in a region from 470nm to 630nm. Within the error the β value is constant. This is also expected in this small spectral range. In further experiments the wavelength range will be extended to the UV and the NIR, so that spectral features of the material or morphology-dependent resonances can be detected.

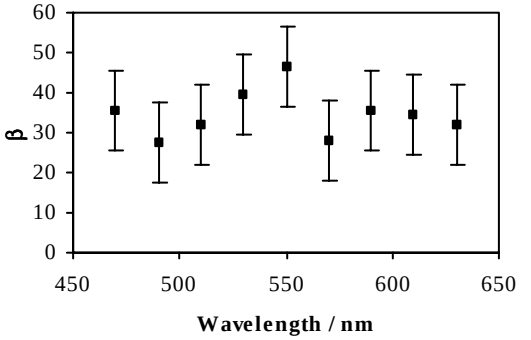

Fig 2. Measured β values as a function of the wavelength for the same graphite particle as in Fig 1.

Further studies are in progress to compare these results on graphite aggregates with other samples.

Acknowledgement: This work is funded by the Deutsche Forschungsgemeinschaft (DFG).

References: [1] Burns J.A. et al. (1979) *Icarus, 40*, 1-48. [2] Mukai T. et al. (1992) *A&A, 262*, 315-320. [3] Kimura H. et al. (2002) *Icarus*, *157*, 349-361. [4] Il'in V.B. and Voshchinnikov N.V. (1998) *A&S SS, 128*, 187-196. [5] Saklayen M.A. and Mukai T. (2004) *Earth Planets Space, 56*, 613-620. [6] Saija R. et al. (2005) *JQSRT, 94*, 163-179. [7] Krauß O. and Wurm G. (2004) *JQSRT, 89*, 179-189. [8] Krauß O. and Wurm G. (2004) *LPS XXXV*, Abstract #1526.

PHYSICS OF DEBRIS DISKS. Alexander V. Krivov[1], [1]Astrophysical Institute and University Observatory. Friedrich Schiller University, Schillergäßchen 2-3, 07745 Jena, Germany, krivov@astro.uni-jena.de.

Introduction: Debris disks are solar system-sized, optically thin, gas-poor dust disks around main-sequence (MS) stars. Their origin and status can easily be understood in the framework of the conventional planetary system formation scenario. Planetesimals, planetary embryos, and then planets form in a primordial protoplanetary disk around a star. A fraction of planetesimals – those that were neither used to make up planets nor ejected – survive this relatively rapid process (1-10 Myr). These left-overs begin to produce dust by mutual collisions and, possibly, comet-type activity [1,2], creating a tenuous debris disk. Being continuously replenished by small bodies, the disk can then persist over much of the star's lifetime.

Although only about a dozen of disks have been resolved so far at different spectral ranges from visual to sub-mm, many more images are expected from ongoing ground-based and space-based searches. Surveys reveal infrared excesses in spectra of hundreds of MS stars and show that at least 15% of MS stars may possess debris disks [3]. Ironically, the "debris disk of the Sun" (dust disk presumably encompassing the Kuiper belt, whose extensions, mass, and cross section area should by far supersede those of the zodiacal cloud) has not been observed yet, due to its extremely low optical depth, typical of Gyr-old systems such as the Sun.

Importance of debris disks stems not only from the fact that they must be a typical constituent of young and mature planetary systems. Due to large total cross section area, dust is much easier to observe than planets. On the other hand, dust distributions reflect distributions of the parent bodies, and are sensitive to presence of embedded perturbers. Hence debris disks can be used as indicators of directly invisible small body populations and tracers of alleged planets.

Interpretation of the rapidly growing bulk of observational data necessitates a major theoretical effort to understand the disk's physics and evolution. This review outlines main physical mechanisms acting in debris disks and their essential properties.

Unperturbed Debris Disks: Parent bodies steadily supply the disk with solids. Initially, most of the mass is released as larger meteoroids, which then undergo collisional grinding. Subsequent evolution of dust-sized particles (<1mm) is largely controlled by three players: stellar gravity, radiation pressure forces, and mutual collisions. Their relative importance depends primarily on the disk's optical depth τ which, in turn, is correlated with system's age.

Observations reveal a nearly linear decay of debris disks with time: τ reduces from ~10^{-2} for Myr-old stars to ~10^{-7} for Gyr-old ones. The phenomenon is naturally explained by collisional depletion of dust parent body populations [4,5]. In old systems with roughly $\tau<10^{-5}$, exemplified by the solar system's debris disk, the Poynting-Robertson (P-R) effect causes migration of smaller grains toward the primary star where they evaporate, while larger grains are typically lost to mutual collisions [6]. If $\tau>10^{-5}$ (all observable extrasolar disks), P-R drag is inefficient [7], as the collisional lifetimes are much shorter than the P-R times. In contrast to protoplanetary disks, collisions in debris disks are destructive and create smaller fragments. Removal of fine debris by stellar radiation pressure is a main loss "channel" of material in such systems. All loss mechanisms listed here imply grain lifetimes of <1Myr, showing that debris disks cannot be primordial.

At any time, a disk contains two distinct populations of dust: bigger grains that can stay in bound orbits around the star (α–meteoroids) and smaller ones that are placed by stronger radiation pressure in hyperbolic orbits, but are steadily replenished through collisional cascade (β–meteoroids). A boundary between the two populations can be estimated from the ratio of the radiation pressure to gravity [8] and lies typically at ~1μm, depending mainly on the mass and luminosity of the star and optical properties of grains, as well as on typical eccentricities of the dust parent bodies (Fig. 1).

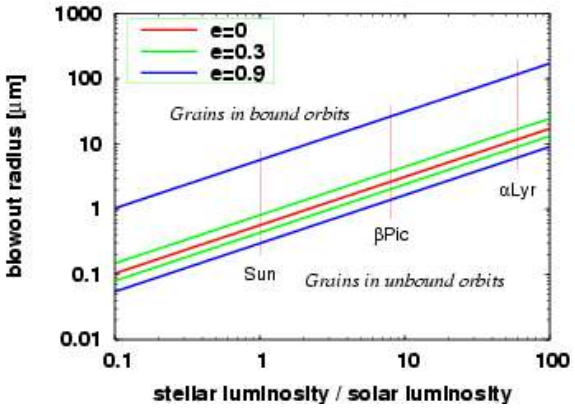

Fig.1. Grain radius that separates particles in bound and hyperbolic orbits, as function of star's luminosity (assuming dust bulk density of 2g/cm^3, a unit radiation pressure efficiency, and a standard mass-luminosity relation for MS stars). Different colors are for different typical eccentricities of parent bodies. Grains between two lines of the same color may be in both types of orbits.

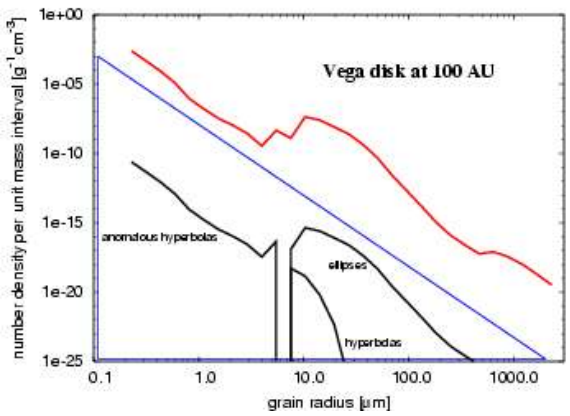

Fig.2. Size distribution in the Vega disk [model, ref. 9]. Triangular inset shows relative contributions to the number density made by grains in bound elliptic orbits, hyperbolic orbits and "anomalous" hyperbolas open outward from the star (orbits of smallest grains, for which radiation pressure exceeds gravity).

A typical size distribution of dust obtained by modeling of the α Lyr disk [9] in depicted in Fig. 2 [see ref. 7 for similar β Pic results]. The total cross section is dominated by particles with radii somewhat above the blowout limit. The entire two-population model provides a good fit to both spectrophotometric and polarimetric data [10].

Not only size distribution, but also spatial distribution of material in the disks must be determined by, and therefore hold the key to, sources, dynamics, and sinks of particles. As a consequence, there exists a principal possibility to constrain properties of the directly invisible small body populations through observations of dust.

Debris disks may contain some gas. In contrast to optically thick young disks around Herbig Ae/Be and T Tau stars, however, the gas density in debris disks is too low to affect the dust dynamics. It may be of some importance only in youngest systems, such as the 12Myr-old β Pic [11], but even this is questionable, because observations aiming to determine the amount of gas yield extremely controversial results [ref. 12 and discussion therein].

Debris Disks Perturbed by Planets: The dust distributions are further complicated by planets that can be embedded in the disk. Many authors studied nonresonant features in the disk arising from secular perturbations (warps and offsets) [13], resonant structures (clumps and voids) [14], and inner gaps resulting from close encounters of dust grains with an alleged planet [15]. All these structures can be directly observable, which offers an indirect method to search for extrasolar planets. Liou and Zook [16] have shown that, were the solar system observed from outside, the presence of at least Neptune and Jupiter could be obvious merely from the analysis of the images of the interplanetary dust disk. Similar research has been done for ε Eri [17], α PsA [18], and other systems. Substructure in the disks is, however, not necessarily produced by presumed planets and may also reflect their intrinsic clumpiness (recent collisions between the large planetesimals). Another problem is that catastrophic grain-grain collisions that may smear out the planet-induced structure already at moderate optical depths [19]. Nevertheless, observations of the fine structure together with dynamical simulations may help to pinpoint unseen planets, even with a moderate mass. These issues are addressed in detail by Moro-Martin (this volume).

Debris Disks as Sources of Interstellar Dust: Recently, radar detection of a stream of dust particles was reported [20], whose source has been identified with β Pic. Observed fluxes and velocities of stream particles are marginally compatible with scenario in which β Pic is a young planetary system that recently passed through an intensive clearance phase by at least one nascent Jupiter [21]. This has reinforced an old discussion [e.g. 22] of whether dust material ejected from debris disks make a perceptible contribution to interstellar dust. There are many reasons to expect that a significant fraction of micron-sized and larger grains in the interstellar medium stem from circumstellar disks [23].

References: [1] Weissman P. R. (1984) *Science, 224,* 987-989. [2] Beust H. et al. (1989) *AAp, 223,* 304-312. [3] Backman D. and Paresce F. (1993) *in Protostar and Planets III, 224,* 1253-1304. [4] Dominik C. and Decin G. (2003) *ApJ, 598,* 626-635. [5] Krivov A. V. et al. (2005) *Icarus, 174, 105-134.* [6] Grün E. et al. (1985) *Icarus, 62,* 244-272. [7] Krivov A. V. et al. (2000) *AAp, 362,* 1127-1137. [8] Burns, J. A. et al. (1979) *Icarus, 40,* 1-48. [9] Krivov A. V. and Loehne T. (2005) *in prep.* [10] Krivova N. A. et al. (2000) *ApJ, 539,* 424-434. [11] Artymowicz P. (1997) *AREPS, 25,* 175-219. [12] Brandeker A. et al. (2004) *AAp, 413,* 681-691. [13] Mouillet D. et al. (1997) *MNRAS, 292,* 896-904. [14] Kuchner M. J. and Holman M. J. (2003) *ApJ, 588,* 1110-1120. [15] Scholl,, H. et al. (1993) *Cel. Mech., 56,* 381—393. [16] Liou J.-C. and Zook H. A. (1999) *AJ, 118,* 580-590. [17] Quillen, A. C. and Thorndike S. (2002) *ApJ, 578,* L149-L152. [18] Holland W. S. et al. (2002) *ApJ, 582,* 1141-1146. [19] Lecavelier des Etangs A. et al. (1996) *Icarus, 123,* 168-179. [20] Baggaley, W. J. (2000) *JGR, 105,* 10,353-10,362. [21] Krivov A. V. et al. (2004) *AAp, 417,* 341-352. [22] Dorschner J. (1967) *Astron. N., 290,* 171-181. [23] Grün E. and Landgraf M. (2000) *JGR, 105,* 10,291-10,297.

Dust Stream Measurements from Ulysses' Distant Jupiter Encounter

H. Krüger[1,2], G. Linkert[2], D. Linkert[2], B. Anweiler[2], E. Grün[2,3] and the Ulysses dust science team

1) Max-Planck-Institut für Sonnensystemforschung, D-37191 Katlenburg-Lindau
2) Max-Planck-Institut für Kernphysik, Postfach 103980, D-69029 Heidelberg,
3) HIGP, University of Hawaii, Honolulu, HI 96822, USA

In 1992 the impact ionisation dust detector on board the Ulysses spacecraft discovered periodic burst-like streams of dust particles within 2 AU from Jupiter. The streams occurred at approximately monthly intervals (28 ± 3 days) and the maximum impact rates exceeded, by three orders of magnitude, the rates typically measured in interplanetary space [3]. These fluctuations were a complete surprise because no periodic phenomenon for small dust particles in interplanetary space was known before. The dust streams gave a completely new picture of interplanetary dust because they showed for the first time that dust originating from the environment of a planet can reach interplanetary space. The particles arrived at Ulysses in collimated streams radiating from close to the line of sight to Jupiter, suggesting a jovian origin. The 28-day periodicity was explained by the particle interaction with the interplanetary magnetic field [4]. Derived particle sizes were ~ 10 nm and the particle speeds exceeded $200\,\mathrm{km\,s^{-1}}$ [6]. With such high speeds, the jovian system turned out to be a source for interplanetary and even interstellar dust. Later Galileo measurements showed strong particle interaction with Jupiter's magnetosphere [5, 2] and Io was identified as the grain source [1].

12 years after its initial Jupiter flyby Ulysses approached the planet a second time in February 2004 with a closest approach distance of 0.8 AU. The first dust stream was detected in November 2002 at a distance of 3.3 AU from Jupiter which was the most distant stream detected so far. The maximum impact rates, measured around equatorial plane crossing of Jupiter, were three times larger than in 1992 (Figure 1). At least 17 dust streams were detected by December 2004, confirming grain properties recognised during the first flyby. The measured impact directions are consistent with a grain origin from the jovian system. The streams occur at about 26 day intervals closely matching the solar rotation period. Close to the equatorial plane the streams occur at a 13 day period, in agreement with theoretical predictions [4]. The impact direction of the streams is correlated with the polarity and strength of the interplanetary magnetic field. Taken all dust stream measurements since 1992 collected with three spacecraft together (Ulysses, Galileo, Cassini) the streams were detected over a large latitude range from the equator to the polar regions of Jupiter ($-35°$ to $+75°$ jovigraphic latitude).

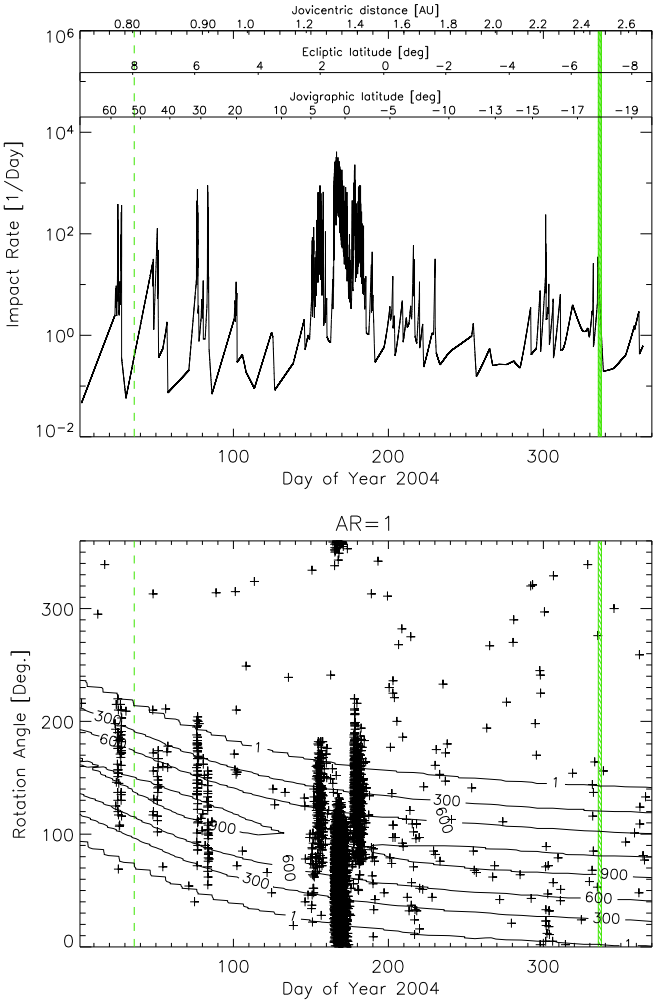

Figure 1: Ulysses dust stream measurements of 2004. *Top:* Impact rate. *Bottom:* Impact direction (spacecraft rotation angle at dust impact; ecliptic north is at 0°). Contour lines show the effective sensor area for particles approaching from the line-of-sight direction to Jupiter. A vertical dashed line shows Jupiter closest approch in February and the shaded area indicates a short period in late November 2004 when the dust instrument was switched off. The distance from Jupiter, ecliptic latitude and latitude with respect to Jupiter are shown at the top.

References

[1] A. L. Graps et al. Io as a source of the Jovian dust streams. *Nature*, 405:48–50, 2000.

[2] E. Grün et al. Galileo observes electromagnetically coupled dust in the Jovian magnetosphere. *Journal of Geophysical Research*, 103:20011–20022, 1998.

[3] E. Grün, et al. Discovery of Jovian dust streams and interstellar grains by the Ulysses spacecraft. *Nature*, 362:428–430, 1993.

[4] D. P. Hamilton and J. A. Burns. Ejection of dust from Jupiter's gossamer ring. *Nature*, 364:695–699, 1993.

[5] M. Horányi, E. Grün, and A. Heck. Modeling the Galileo dust measurements at Jupiter. *Geophysical Research Letters*, 24:2175–2178, 1997.

[6] H. A. Zook, et al. Solar wind magnetic field bending of Jovian dust trajectories. *Science*, 274:1501–1503, 1996.

Galileo In-Situ Dust Measurements in Jupiter's Gossamer Rings

H. Krüger[1,2], R. Moissl[1,2], D. P. Hamilton[3] E. Grün[2,4]

1) Max-Planck-Institut für Sonnensystemforschung, D-37191 Katlenburg-Lindau
2) Max-Planck-Institut für Kernphysik, Postfach 103980, D-69029 Heidelberg,
3) Department of Astronomy, University of Maryland, College Park, MD 20742-2 421, USA
4) HIGP, University of Hawaii, Honolulu, HI 96822, USA

Jupiter's ring system – the archetype of ethereal planetary ring systems – consists of at least three components: the main ring, the vertically extended halo and the gossamer ring(s). The small moonlets Thebe and Amalthea orbit Jupiter within the gossamer ring region, and structure in the intensity obtained from imaging observations indicates that these moons are the dominant sources of the gossamer ring material. Typical grain radii derived from imaging are a few microns. The current picture implies that particles ejected from a source moon evolve inward under Poynting-Robertson drag [1]. Beyond Thebe's orbit, a very faint outward extension of the gossamer ring was also observed which is not yet explained.

The Galileo spacecraft traversed the gossamer rings in November 2002 and September 2003, and the in-situ dust detector on board [3] collected dust measurements during both ring passages. These are the first in-situ measurements in a 'dusty' planetary ring which was also studied with imaging techniques. In-situ dust measurements provide information about the physical properties of the dust environment not accessible with imaging techniques. In particular, they provide dust spatial densities along the spacecraft trajectory as well as grain sizes and impact speeds.

Several thousand dust impacts were recorded during both ring traverses. The measurements reveal a gap in the dust spatial density between Amalthea's and Thebe's orbits (Figure 1) which is a previously unrecognised structure in the gossamer rings. The impact rate strongly increases in the Amalthea gossamer ring, consistent with imaging results. The measured size distribution of the grains ranges from 0.2 to 3 μm [6], extending by an order of magnitude the size distribution towards smaller particles is than accessible with optical techniques.

A shadow resonance, first investigated by [5], naturally explains gaps of material interior to Thebe's orbits and also explains the outward extension of the ring beyond the orbit of that satellite [4]. When a dust grain enters Jupiter's shadow, photoelectric charging by solar radiation switches off, and the grain's electric potential decreases. This changes the electromagnetic force acting on the particle and results in coupled oscillations of the orbital eccentricity and semimajor axis. These oscillations cause the rings to extend significantly outward, but only slightly inward, of their source moons while preserving their vertical thicknesses. This is exactly what is observed for the Thebe ring extension. The model leads to longitudinally asymmetric gossamer rings offset away from the Sun for positive grain charges. If most ring material is reabsorbed by the satellites before drag forces can draw it inward, this would create the gap interior to Thebe that is visible in the rate plot in Figure 1.

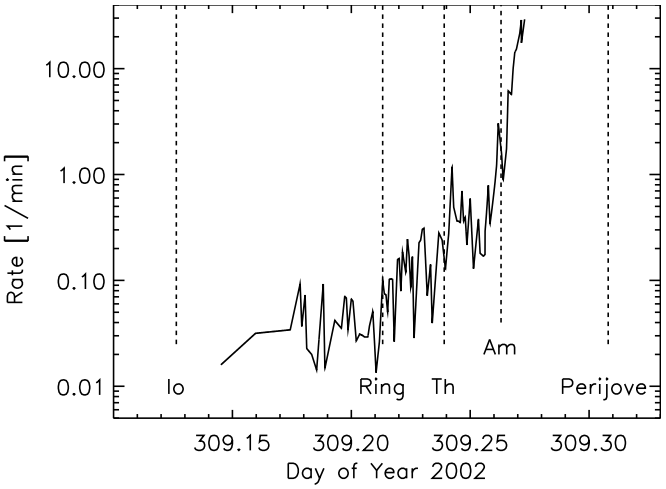

Figure 1: Impact rate of the smallest (sub-micron) dust particles (impact charges $Q_I < 10^{-13}$ C) at Galileo's gossamer ring passage in November 2002 (A34). Dotted vertical lines indicate the locations of the edge of the outer extension of the ring beyond Thebe's orbit seen on ring images at 3.75 R_J (Ring, Jupiter radius R_J = 71492 km), Thebe's orbit (Th, 3.11 R_J), and Amalthea's orbit (Am, 2.54 R_J). The spatial resolution is about 1100 km in radial direction. Note the strong dip between Thebe's and Amalthea's orbits. A similar dip also appears on ring images [2] but remains controversial .

References

[1] J. A. Burns et al. The formation of Jupiter's faint rings. *Science*, 284:1146–1150, 1999.

[2] I. De Pater et al. Keck Infrared Observations of Jupiter's Ring System near Earth's 1997 Ring Plane Crossing. *Icarus*, 138:214–223, 1999.

[3] E. Grün et al. The Galileo dust detector. *Space Science Reviews*, 60:317–340, 1992.

[4] D. P. Hamilton. Jupiter's Gossamer Rings Explained. *Bulletin of the American Astronomical Society*, 2003. Abstract presented at the DPS conference 2003.

[5] M. Horányi and J. A. Burns. Charged dust dynamics - Orbital resonance due to planetary shadows. *Journal of Geophysical Research*, 96:19283–19289, 1991.

[6] H. Krüger. *Jupiter's Dust Disc, An Astrophysical Laboratory*. Shaker Verlag Aachen, ISBN 3-8322-2224-3, 2003. Habilitation Thesis Ruprecht-Karls-Universität Heidelberg.

CASSINI RPWS OBSERVATIONS OF DUST IMPACTS IN SATURN'S E-RING. W. S. Kurth[1], T. F. Averkamp[1], D. A. Gurnett[1], and Z. Z. Wang[1], [1]Dept. of Physics & Astronomy, The University of Iowa, Iowa City, IA 52242; William-kurth@uiowa.edu.

Introduction: The Cassini radio and plasma wave science (RPWS) instrument observes signatures of micron-sized particles impacting the spacecraft which can provide information on spatial variations of the number density of dust particles in Saturn's E-ring and estimates of their masses. Preliminary results show that there is a local maximum of the number density of dust particles near the orbit of Enceladus with a thickness of about 5000 km (full width at half-maximum count rate). Preliminary estimates of the sizes of the impacting particles are a few microns.

Technique: The RPWS observes a voltage pulse at the input to its electric preamplifier that is due to a small dust particle impacting the spacecraft at speeds of order 10 km/s [1]. The impacting particle has sufficient kinetic energy to vaporize both itself and a small portion of the target material, resulting in a gas with temperatures of order 10^5 K. This temperature is high enough to ionize a significant fraction of the vapor, resulting in a rapidly-escaping electron cloud and a resulting time-variable electric field. If the impact rate is very high, the electric field spectrum will have an f^{-4} dependence. This was the case during crossings through the gap between the F- and G-rings before and after Saturn orbit insertion [1, 2] with impact rates of ~ 1000 s^{-1}. This f^{-4} spectrum allows an estimate of the rms mass of the impacting particles [2,3]. In the E-ring, however, the impact rate is only a few 10's s^{-1}, and shot noise (due to electrons moving past the antennas) dominates the high-frequency spectrum [3]. Here, we must rely on individual detections of the impacts using wideband waveforms that show the voltage pulses.

The individual impacts are found by analyzing temporal variations of the antenna potential appearing similar to those shown in Figure 1. This is best done on the ground, but requires that large data volumes be transmitted to the ground, as the wideband data is generated at rates of 10's of kbps or more, hence, the amount of time for which these data can be acquired is limited. The RPWS also has an on-board algorithm designed to detect the signature of dust impacts from the same waveform data, but the algorithm is limited by its simplicity and has a large effective threshold, limiting it to the largest particles and impact rates of only a few s^{-1}.

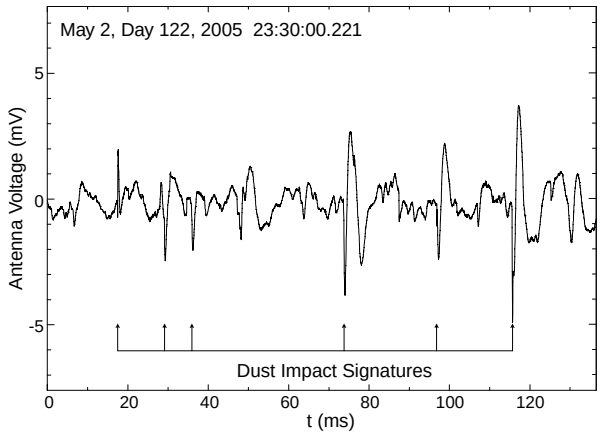

Figure 1: Examples of dust impact signatures.

Preliminary Results: In equatorial passes, impact rates peak near the orbit of Enceladus, suggesting a local source for E-ring particles at this location. Non-equatorial passes through the equator near the orbit of Enceladus allow for a measurement of the thickness of the E-ring at this location. Figure 2 shows the impact rate profile for one such pass on Cassini's 7th orbit of Saturn. The peak impact rate is about 50 s^{-1}. While there is some structure in the profile near its peak which is not currently understood, the remaining portion of the profile is well fit by a Gaussian distribution with a scale height of 2800 km. This translates to a full width at half-maximum of the order of 5000 km.

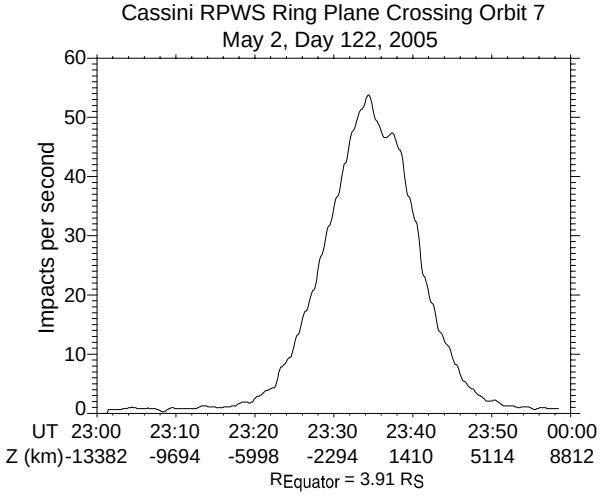

Figure 2: Impact rate profile for Orbit 7 ring plane crossing near the orbit of Enceladus

Knowing the relative impact speed v and an estimate for the cross-sectional area A of the spacecraft, we can calculate a number density n for the detected particles from the impact rate R using $n = R/vA$. The true cross-sectional area of relevance to this problem is likely a complicated function of the projected areas of different materials (which have different yields when impacted by a high velocity particle). For simplicity, we take the area of the 4-m diameter high gain antenna 12.6 m^2 for A. For the Orbit 7 ring plane crossing, the relative speed between the spacecraft and dust v (assuming circular Keplarian orbits) is 8 km/s. So, using the peak impact rate of 50 s^{-1}, the peak number density is approximately 5 x 10^{-4} m^{-3}.

While it is almost certainly true that the amplitude of the voltage pulse measured for a given impact is proportional to the mass of the impacting particle, there are numerous complicating factors that make it difficult to accurately determine the mass. For this work, we utilize the results of Wang et al. [2] who have used the method of Aubier et al. [3] to determine the root mean square mass m of particles detected during two crossings of the ring plane in the gap between the F- and G-rings near the time of Cassini's orbit insertion. The voltage V produced by an impact is $V = k m v^{\beta}$ where k is a constant. The value for β is determined experimentally and is somewhat uncertain, but we use 3.2 given by Adams and Smith [4]. The impact speed for the measurements between the F- and G-rings is approximately 16 km/s, or a factor of two larger than for the Orbit 7 E-ring crossing. Simply taking the ratio of the expressions for the rms voltages determined by Wang et al. and those determined here for the E-ring and using the Wang et al. rms mass of ~ 5 x 10^{-11} g, we estimate the E-ring rms mass to be approximately 2 x 10^{-10} g. This corresponds to ice spheres of radius of a few microns. This estimate is larger than those determined for the E-ring in general of 1 micron [cf. 5]. We emphasize that the preliminary nature of our size estimate and the large uncertainties in the analysis of the impacts leading to this size. However, it may also be the case that these particles which we see preferentially near the orbit of Enceladus are actually larger and represent parent bodies for the E-ring population.

We are currently attempting to cross-calibrate these mass determinations with measurements by the Cosmic Dust Analyzer on Cassini. However, it is too soon to know whether or by how much the mass determined by the above impact analysis will change.

References: [1] Gurnett, D. A. et al. (2005) *Science, 307,* 1255–1259. [2] Wang, Z. Z. et al. (2005) *Planet. Space Sci.,* in preparation. [3] Aubier, M. G., Meyer-Vernet, N., and Pedersen, B. M. (1983) *GRL, 10,* 5-8. [4] Adams, N. G., and Smith, D. (1971) *Planet. Space Sci.*, *19*, 195-204. [5] Showalter, M. R., Cuzzi, J. N., and Larson, S. M., (1991) *Icarus*, *94*, 451-473.